Stochastic reaction and diffusion on growing domains: Understanding the breakdown of robust pattern formation

Thomas E. Woolley,[1,*] Ruth E. Baker,[1] Eamonn A. Gaffney,[1] and Philip K. Maini[1,2]

[1]*Centre for Mathematical Biology, Mathematical Institute, University of Oxford, 24-29 St Giles', Oxford OX1 3LB, United Kingdom*

[2]*Oxford Centre for Integrative Systems Biology, Department of Biochemistry, University of Oxford, South Parks Road OX1 3QU, United Kingdom*

(Received 15 June 2011; published 28 October 2011)

Many biological patterns, from population densities to animal coat markings, can be thought of as heterogeneous spatiotemporal distributions of mobile agents. Many mathematical models have been proposed to account for the emergence of this complexity, but, in general, they have consisted of deterministic systems of differential equations, which do not take into account the stochastic nature of population interactions. One particular, pertinent criticism of these deterministic systems is that the exhibited patterns can often be highly sensitive to changes in initial conditions, domain geometry, parameter values, etc. Due to this sensitivity, we seek to understand the effects of stochasticity and growth on paradigm biological patterning models. In this paper, we extend spatial Fourier analysis and growing domain mapping techniques to encompass stochastic Turing systems. Through this we find that the stochastic systems are able to realize much richer dynamics than their deterministic counterparts, in that patterns are able to exist outside the standard Turing parameter range. Further, it is seen that the inherent stochasticity in the reactions appears to be more important than the noise generated by growth, when considering which wave modes are excited. Finally, although growth is able to generate robust pattern sequences in the deterministic case, we see that stochastic effects destroy this mechanism for conferring robustness. However, through Fourier analysis we are able to suggest a reason behind this lack of robustness and identify possible mechanisms by which to reclaim it.

DOI: 10.1103/PhysRevE.84.046216 PACS number(s): 89.75.Kd, 82.20.Uv, 82.39.−k, 82.40.Ck

I. INTRODUCTION

Mathematical modeling is of fundamental importance in developmental biology due to its ability to suggest and test mechanisms by which complex biological patterns can arise [1]. Although many mechanisms have been proposed [2–6], we focus on the Turing system as a model of morphogenesis [7–9] as it has been postulated to be the key mechanism behind feather bud, limb bud, and hair follicle development [1,10–13]. In most cases these models have been constructed in a deterministic framework and the effects of intrinsic noise on pattern formation have only recently been considered [14]. Indeed, due to the sensitivity of the Turing model to perturbations in parameter values, domain geometry, etc., it has been seen that stochastic effects are able to influence the evolving patterns in ways not seen through deterministic simulations [14].

Previous research in the area of stochastic reaction-diffusion systems has focused on analyzing and simulating the effects of external noise [15–19]. External noise is modeled as an additional effect that is controlled by the user, thus its properties are known *a priori*. Here, we focus on the role of intrinsic stochasticity by modeling diffusion of the chemical constituents as a space-jump process [20], i.e., the individual particles of the chemical populations undergo unbiased random walks on a domain which has been discretized into boxes. Reactions between constituent populations are assumed to act within each box, thus reagents in box i can only react with other reagents in box i. For each stochastic system, a chemical master equation (CME) can be generated as an exact description of the evolution of the system [21]. Linear noise expansions allow derivation of Fokker-Plank equations that characterise the properties of the noise, which can then be converted into ordinary differential equations (ODEs) that define the covariances [22]. Recently developed spatial Fourier transform techniques [23–29] can also be applied in order to gain an insight into the potential spatial dynamics that are possible in such systems.

Primarily, we can consider which wave modes are stochastically excited inside and outside of the deterministic Turing domain. Within the parameter region that allows deterministic systems to realize Turing patterns, we analytically demonstrate that the stochastically excited wave modes correspond exactly to their deterministic analogues. It is found that these stochastically excited wave modes grow exponentially with time and, since the noise perturbs the populations away from the uniform steady state, patterning is able to form much earlier in a stochastic system than in its deterministic counterpart. Outside of this region, deterministic systems are unable to sustain viable patterns, whereas the noise inherent in a stochastic system is able to produce a state that is consistently far removed from the homogeneous steady state, a result that was previously noted by Biancalani *et al*. [14].

Having considered the stationary domain case, we use a recently developed mapping technique [28,29] to explore stochastic reaction-diffusion systems on growing domains. We are interested in the effects of stochasticity in such systems, as, in the deterministic setting, it has been shown that domain growth is able to support robust pattern doubling sequences [30]. Barrass *et al*. [32] further illuminated this mechanism by producing bifurcation diagrams showing the observed pattern doubling occurs by the mth wave mode destabilizing and

*woolley@maths.ox.ac.uk

the solution trajectory moving onto the stabilized $2m$ wave mode. During the jump from one stable mode to the other, the trajectory moves through a window where wave modes k, $m < k < 2m$, may also be stable, thus, if the growth is too slow, period doubling will break down. Alternatively, if growth is too fast, period doubling breaks down because the system does not reside for sufficiently long in a specific range of pattern stability to allow that pattern to establish [31]. Furthermore, in the case that domain length has a more complex dependence on concentration, growth can cause a number of interesting pathological phenomena [31].

We cast the Turing models onto growing domains in order to consider the possible transition sequences. Since robustness in a deterministic Turing system is achieved through domain growth, we may naïvely suspect that robustness may also exist in the stochastic formulation, since the excited wave modes are identical in both systems. However, it is quickly realized that stochasticity inhibits pattern-doubling robustness. Even in the limit of large populations, stochasticity is able to cause a breakdown in the doubling, eventually. Although we lose period doubling as a mechanism of robustness, stochastic systems appear to excite consecutive modes, and thus we investigate the robustness of this mechanism through simulation.

With the aim of analyzing robustness, or lack thereof, in mind, we start in Sec. II by creating the stochastic framework in which we will construct the models. In Sec. III we justify the mapping from the Eulerian domain, which is time-dependent, to the Lagrangian domain, which is time-independent, and then recapitulate the application of spatial Fourier transforms on growing domains in Sec. IV. The effects of stochasticity on a specific Turing system, both inside and outside of the Turing unstable parameter region, are then considered in Sec. V, and these results are then extended to the case of deterministically and stochastically growing domains. Finally, in Sec. VI, we show that the stochastically excited wave modes are exactly equivalent to their deterministic analogues and derive an inequality for the discretization needed to generate noise appropriately.

II. STOCHASTIC FORMALISM

For a detailed discussion of the following ideas see Refs. [28,29], where we considered a general system containing a single stochastic biochemical population. In order to examine Turing systems, we need to consider at least two spatially extended populations that interact through nonlinear reactions. Thus, in this section, we briefly recapitulate the weak noise expansion, applied to a system of two diffusing populations, $U(x,t)$ and $V(x,t)$, that are coupled through nondelayed reactions, on a one-dimensional domain.

Although other descriptions of diffusion are possible [33], we model diffusion as a space-jump process; see Fig. 1 [20]. The domain is partitioned into one-dimensional boxes of size Δ_E, where each box, i, contains the indexed populations, U_i and V_i. Higher dimensional domains can be considered by replacing the one-dimensional boxes with appropriate analogues [34]. Thus, for two particle types that have been discretized into K compartments in a one-dimensional domain

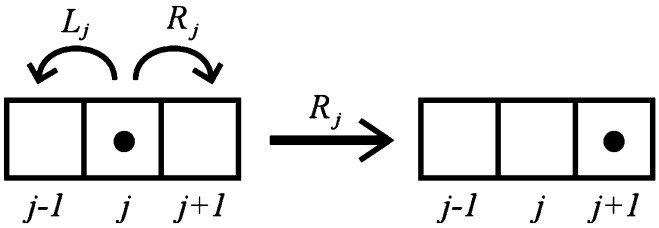

FIG. 1. Diagram illustrating the stochastic description of diffusion. Each particle has equal probability of moving left as of moving right. If, for example, the right diffusion reaction, R_j, occurs one molecule from box j moves to box $j+1$. Reproduced from Ref. [28]. "Copyright 2011 by the American Physical Society."

of length L, with Neumann boundary conditions and stochastic diffusion coefficients d_u and d_v, respectively, the diffusion reactions are:

$$U_1 \underset{d_u}{\overset{d_u}{\rightleftharpoons}} U_2 \underset{d_u}{\overset{d_u}{\rightleftharpoons}} \cdots \underset{d_u}{\overset{d_u}{\rightleftharpoons}} U_K, \tag{1}$$

$$V_1 \underset{d_v}{\overset{d_v}{\rightleftharpoons}} V_2 \underset{d_v}{\overset{d_v}{\rightleftharpoons}} \cdots \underset{d_v}{\overset{d_v}{\rightleftharpoons}} V_K. \tag{2}$$

We use U_i and V_i to stand for both respective species and populations and this abuse of notation should not cause confusion. Since a space-jump process gives rise to first-order reactions, the equations governing mean particle numbers are equivalent to the equations derived using the Law of Mass Action [35]. Thus, if $d_u = D_u/\Delta_E^2$ and $d_v = D_v/\Delta_E^2$, where D_u and D_v are the macroscopic rates of diffusion [36], then the mean-field equations are seen to be second-order, finite difference approximations of the one-dimensional Laplacian, which is derived through a Taylor expansion of the continuous formulation [37,38].

In addition to diffusion, suppose these populations undergo J reactions, $\{R_1,\ldots,R_J\}$. For simplicity, we use the convention that bold variables stand for the vector of spatially extended variables, e.g. $\boldsymbol{U}(t) = [U_1(t),\ldots,U_K(t)]$ and $\boldsymbol{V}(t) = [V_1(t),\ldots,V_K(t)]$ are the state vectors of the system at time t. Each reaction, R_j, is specified by the propensity function, $a_j(\boldsymbol{u},\boldsymbol{v})$, where $\boldsymbol{u}$ and $\boldsymbol{v}$ are single realizations of $\boldsymbol{U}$ and $\boldsymbol{V}$ and the stoichiometric vector $\boldsymbol{\nu}_j = (\nu_{1j},\ldots,\nu_{2Kj})$. Explicitly, for the jth reaction, ν_{ij} is the change in population U_i for $1 \leqslant i \leqslant K$ and V_{i-K} for $K+1 \leqslant i \leqslant 2K$. From these definitions and the Laws of Probability [39], we can construct the CME. By defining $P(\boldsymbol{W},t) = P(\boldsymbol{u},\boldsymbol{v},t)$ to be the probability of being in state $\boldsymbol{W} = (\boldsymbol{u},\boldsymbol{v})$ at time t, then, given an initial state, $\boldsymbol{W}_0 = (\boldsymbol{U}(t_0),\boldsymbol{V}(t_0)) = (u_0,v_0)$,

$$\frac{\partial}{\partial t}P(\boldsymbol{W},t|\boldsymbol{W}_0,t_0) = \sum_{j=1}^{J}[P(\boldsymbol{W}-\boldsymbol{\nu}_j,t|\boldsymbol{W}_0,t_0)a_j(\boldsymbol{W}-\boldsymbol{\nu}_j) - P(\boldsymbol{W},t|\boldsymbol{W}_0,t_0)a_j(\boldsymbol{W})]. \tag{3}$$

Due to the CME usually being nonlinear it is generally not solvable, except in certain, special, circumstances [37, 40]. Thus, we derive a weak noise expansion of the CME using a suitable system parameter, denoted Ω. This expansion allows us to consider the deterministic and stochastic effects separately.

We define new random variables, η_{ui} and η_{vi} (which are of order one as $\Omega \to \infty$), for $i = 1, \ldots, K$, through the relations,

$$U_i = \phi_i \Omega + \eta_{ui} \sqrt{\Omega}, \tag{4}$$

$$V_i = \psi_i \Omega + \eta_{vi} \sqrt{\Omega}, \tag{5}$$

where Ω is the magnitude of the smallest homogeneous steady state of the populations $\boldsymbol{U}$ or $\boldsymbol{V}$. ϕ_i and ψ_i are the expected ratios of the populations at time t to the order of magnitude, Ω, and are dimensionless "macroscopic" variables. The statistics of U_i and V_i are linked to η_{ui} and η_{vi}, respectively, through the identification [22]

$$P(\boldsymbol{U}, \boldsymbol{V}, t) = \Pi(\boldsymbol{\eta_u}, \boldsymbol{\eta_v}, t). \tag{6}$$

By using this form of expansion the fluctuations are treated as Gaussian perturbations about the deterministic solution and, as such, this approximation only works in the case of large Ω. Note that, if considering a monotonically increasing process, such as exponential growth, this approximation suggests that, although the mean population undergoes a net exponential growth, the domain length in the Gaussian approximation is able to shrink instantaneously. The final piece of terminology we need is the macroscopic rate of reaction, a_j, which is used to define the macroscopic variables, ϕ_i and ψ_i, as solutions of

$$\frac{d\phi_i}{dt} = \sum_{j=1}^{J} \mathsf{a}_j(\boldsymbol{\phi}, \boldsymbol{\psi}) \nu_{ij}, \tag{7}$$

$$\frac{d\psi_i}{dt} = \sum_{j=1}^{J} \mathsf{a}_j(\boldsymbol{\phi}, \boldsymbol{\psi}) \nu_{(K+i)j}. \tag{8}$$

Through using the relationships between P, Π, a_j, and a_j, we are able to expand and separate Eq. (3) in terms of decreasing orders of Ω [28,29]. The leading order terms are of size $\mathcal{O}(\sqrt{\Omega})$ and define the deterministic dynamics of the macroscopic equations,

$$\sum_{i=1}^{K} \left[\frac{d\phi_i}{dt} \frac{\partial \Pi}{\partial \eta_{ui}} + \frac{d\psi_i}{dt} \frac{\partial \Pi}{\partial \eta_{vi}} \right] = \sum_{j=1}^{J} \left[\sum_{i=1}^{K} \mathsf{a}_j(\boldsymbol{\phi}, \boldsymbol{\psi}) \nu_{ij} \frac{\partial \Pi}{\partial \eta_{ui}} + \sum_{i=1}^{K} \mathsf{a}_j(\boldsymbol{\phi}, \boldsymbol{\psi}) \nu_{K+ij} \frac{\partial \Pi}{\partial \eta_{vi}} \right]. \tag{9}$$

This is satisfied by the definitions of ϕ_i and ψ_i in Eqs. (7) and (8).

The second-order term in the expansion is of size $\mathcal{O}(1)$ and gives rise to a Fokker-Planck equation [41], which defines the dynamics of the probability density,

$$\frac{\partial \Pi}{\partial t} = -\sum_{i,l=1}^{2K} A_{il} \frac{\partial [\eta_l \Pi]}{\partial \eta_i} + \frac{1}{2} \sum_{i,l=1}^{2K} B_{il} \frac{\partial^2 \Pi}{\partial \eta_i \partial \eta_l}, \tag{10}$$

where $\eta_i = \eta_{ui}$ for $i = 1, \ldots, K$ and $\eta_i = \eta_{vi-K}$ for $i = K + 1, \ldots, 2K$. The coefficients A_{il} and B_{il} are defined through the matrix equations [42]

$$\boldsymbol{A} = \{A_{il}\} = \{\partial [\boldsymbol{\nu} \mathsf{a}]_i / \partial \phi_l\}, \tag{11}$$

$$\boldsymbol{B} = \{B_{il}\} = \boldsymbol{\nu} \mathrm{diag}(\mathsf{a}) \boldsymbol{\nu}^T, \tag{12}$$

$$\boldsymbol{\nu} = \{\nu_{ij}\}_{i=1,\ldots,K}^{j=1,\ldots,J}, \tag{13}$$

and $\mathsf{a}^T = (\mathsf{a}_1, \ldots, \mathsf{a}_J)$.

III. LAGRANGIAN COORDINATES

As discussed in Sec. I, growth has been used theoretically to ensure robustness in deterministic Turing patterning systems [30]. Because growth is so important in biology [43], there has recently been interest in producing a stochastic description of growth [20] that is consistent with continuum theory [44].

In previous work [28,29], we developed a rigorous analytic framework that allows the consideration of stochastic and deterministic domain growth by mapping the growing Eulerian domain to a static Lagrangian domain. This consists of discretizing a domain into K boxes, as usual, but each box, i, is now identified as a Lagrangian compartment of size Δ_L, containing $N_i(t)$ Eulerian subdivisions of size Δ_E (see Fig. 2). This microscopic variable, $N_i(t)$, is governed by a stochastic process and is linked to a macroscopic variable, $n_i(t)$, which defines the average ratio of Lagrangian box size, Δ_L, to the total size of the corresponding Eulerian subcompartments, $N_i(t)\Delta_E$, at time t. Further, similar to Sec. II, a new random variable, $\epsilon_i(t)$, is defined through

$$N_i = n_i \theta + \epsilon_i \sqrt{\theta}, \tag{14}$$

where

$$\theta \stackrel{\text{def}}{=} \frac{\Delta_L}{\Delta_E}, \tag{15}$$

is the scaling of Eulerian box length to Lagrangian box length. Initially, the $N_i(0)$ are taken to be equal for all i, thus,

$$\Delta_L n_i(0) = \theta \Delta_E = N_i(0) \Delta_E, \tag{16}$$

(see Fig. 2) and hence, $n_i(0) = 1$ for all i. The intrinsic noise in the domain length arises through probabilistic changes in the number of microscopic compartments, which are biologically motivated by the stochastic processes of cell division and cell death. Thus, similar to the case of reactions, the noise forms an integral part of the domain's dynamics.

In the Appendix we use the specific example of Schnakenberg reaction kinetics to illustrate the effect of this spatial mapping. Since the mean-field behaviour of the CME is given by the deterministic system shown in Eqs. (A6) and (A7) we use the deterministic reaction rates to produce stochastic

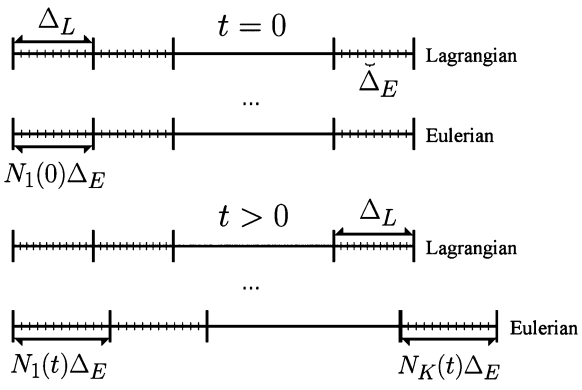

FIG. 2. Illustration of the connection between the Lagrangian description of the domain and the corresponding Eulerian description. See text for details. Reproduced from Ref. [28]. "Copyright 2011 by the American Physical Society."

analogues by substituting $n_i(t)$ for N_i/θ and noting that,

$$\lim_{\theta\to\infty}\frac{N_i(t)}{\theta}=n_i(t). \tag{17}$$

Using the weak noise expansion [22,42] discussed in Sec. II, we can separate the leading order equations of Ω and θ to obtain the deterministic behavior, and then consider the lower-order terms to explore the stochastic behavior. Note that not only do we obtain terms of order one, but there will be new terms of order $\sqrt{\Omega/\theta}$. Thus, the general Fokker-Planck equation for stochastic reactions on a stochastically growing domain is

$$\frac{\partial\Pi}{\partial t}=-\sum_{i,j=1}^{3K}A_{ij}\frac{\partial}{\partial\zeta_i}(\zeta_j\Pi)\sqrt{\frac{\Theta_j}{\Theta_i}}+\frac{1}{2}\sum_{i,j=1}^{3K}B_{ij}\frac{\partial^2\Pi}{\partial\zeta_i\partial\zeta_j}\frac{\Theta_j}{\Theta_i}, \tag{18}$$

where Θ_i is the scaling for the variable ζ_i. In the current case, $\zeta_i=\eta_{ui}$ for $i=1,\ldots,K$; $\zeta_i=\eta_{vi-K}$ for $i=K+1,\ldots,2K$; $\zeta_i=\epsilon_{i-2K}$ for $i=2K+1,\ldots,3K$; $\Theta_i=\Omega$ for $i=1,\ldots,2K$; and $\Theta_i=\theta$ for $i=2K+1,\ldots,3K$. Note that, for simplicity, whenever we consider stochastic growth we fix the scaling parameters to be equal, i.e., $\theta=\Omega$. If $\theta\ll\Omega$, it would be possible to assume that the reactions were deterministic on a stochastically growing domain. However, since we are interested in small particle numbers this is not considered here. Similarly, if $\theta\gg\Omega$, the domain would effectively be growing deterministically. This assumption is used later, once we have compared deterministic and stochastic growth in Sec. V B and shown that the noise generated from growth is much less significant than that generated from reactions. Furthermore, we see that the pattern evolution of a Turing system on a stochastically growing domain is sufficiently similar to one undergoing deterministic growth so that it is appropriate to investigate only deterministic growth. Finally, we fix the form of Lagrangian diffusion to be approximate midpoint to midpoint diffusion [29]. This defines the transition rates left and right to be equal to

$$\frac{d_L}{\frac{1}{\theta^2}N_i^2}, \tag{19}$$

where $d_L=d_u$ or d_v depending on the population. For a derivation of this rate from Dynkin's formula see Refs. [29,45].

In general, a system of nondelayed, coupled reaction-diffusion equations on a deterministically growing domain can be rescaled to remove dilution and projected on to the stationary domain thus giving the form (see the Appendix) [30,43,44]:

$$\frac{\partial\phi}{\partial t}(x,t)=\frac{D_u}{n(t)^2}\nabla^2\phi(x,t)+f[\phi(x,t),\psi(x,t),t], \tag{20}$$

$$\frac{\partial\psi}{\partial t}(x,t)=\frac{D_v}{n(t)^2}\nabla^2\psi(x,t)+g[\phi(x,t),\psi(x,t),t], \tag{21}$$

where $\phi(t)$, $\psi(t)$, and $n(t)$ are the spatially continuous forms of the discretized populations $\phi_i(t)$, $\psi_i(t)$, and $n_i(t)$, respectively. Also, due to the rescaling of the reaction kinetics using $n(t)$ (see the Appendix), the kinetic functions of the reactions, f and g, will normally be time-dependent. Thus, except for the diffusion term (which uses a three-point stencil in one dimension), the discretized system will contain only terms evaluated at the same spatial and temporal points. Further, since we are dealing with a regular grid of points in the discretized domain, the diffusive operator stencil only includes two neighboring spatial terms. These are identical at all points across the domain, excluding the end points, which are accounted for by the form of the Fourier cosine expansion. Thus, the matrices A and B, defined in Eqs. (11) and (12), can be split into symmetric tridiagonal submatrices, where the terms along each diagonal are identical. This allows the equations to be Fourier-transformed analytically, even where we have time-dependent coefficients. If instead an irregular discretization is used, the Fourier transform can be calculated, but only numerically. Although, by considering different stochastic descriptions of diffusion the number of nonzero super- and subdiagonals may change, the matrices will always be symmetric and so spatial Fourier transforms will always be applicable.

For stochastic growth, the matrices $\boldsymbol{A}$ and $\boldsymbol{B}$ will be $3K\times 3K$ in size, as we have three distinct, spatially discretized populations, $\boldsymbol{U}$, $\boldsymbol{V}$, and $\boldsymbol{N}=(N_1,N_2,\ldots,N_K)$. In the case that the growth rate is independent of the chemical concentrations, $\boldsymbol{A}$ and $\boldsymbol{B}$ will have sparse forms. These matrices can be split up into nine $K\times K$ submatrices of the form

$$\boldsymbol{A}=\begin{bmatrix}\boldsymbol{a}&\boldsymbol{b}&\boldsymbol{e}\\ \boldsymbol{c}&\boldsymbol{d}&\boldsymbol{f}\\ \boldsymbol{0}&\boldsymbol{0}&\boldsymbol{0}\end{bmatrix},\quad \boldsymbol{B}=\begin{bmatrix}\boldsymbol{\alpha}&\boldsymbol{\beta}&\boldsymbol{0}\\ \boldsymbol{\beta}&\boldsymbol{\gamma}&\boldsymbol{0}\\ \boldsymbol{0}&\boldsymbol{0}&\boldsymbol{\delta}\end{bmatrix}, \tag{22}$$

where $\boldsymbol{b}$ and $\boldsymbol{c}$ are diagonal and the zeros exist because a change in the number of Eulerian subdivisions, N_i, only affects the chemical species U_i and V_i through the diffusion coefficient. Since we would like to consider stochastic growth the submatrices $\boldsymbol{a}$, $\boldsymbol{d}$, $\boldsymbol{e}$, and $\boldsymbol{f}$ have nonunique forms due to different possible spatial dependencies in the definition of diffusion on a Lagrangian domain [29]. However, as mentioned, in the present case we fix the definition of diffusion to be approximate midpoint to midpoint diffusion, so that the matrices $\boldsymbol{a}$, $\boldsymbol{d}$, $\boldsymbol{e}$, and $\boldsymbol{f}$ will be tridiagonal and symmetric.

For the matrix $\boldsymbol{B}$, we first note that, by definition, it is symmetric and the submatrices $\boldsymbol{\alpha}$, $\boldsymbol{\beta}$, and $\boldsymbol{\gamma}$ are of the same structure as the corresponding submatrices of $\boldsymbol{A}$. The submatrix $\boldsymbol{\delta}$ is diagonal since each growth "reaction" only affects a single Lagrangian box. For a specific worked example of the derivation of $\boldsymbol{A}$ and $\boldsymbol{B}$, see the Appendix.

Using matrices $\boldsymbol{A}$ and $\boldsymbol{B}$, we are able to derive the corresponding general Fokker-Plank equation for the variables η_{ui}, η_{vi}, and ϵ_i:

$$\begin{aligned}\frac{\partial\Pi}{\partial t}=&-\sum_{i,j}\boldsymbol{a}_{ij}\frac{\partial}{\partial\eta_{ui}}[\eta_{uj}\Pi]-\sum_{i,j}\boldsymbol{b}_{ij}\frac{\partial}{\partial\eta_{ui}}[\eta_{vj}\Pi]-\sum_{i,j}\boldsymbol{e}_{ij}\frac{\partial}{\partial\eta_{ui}}[\epsilon_j\Pi]-\sum_{i,j}\boldsymbol{c}_{ij}\frac{\partial}{\partial\eta_{vi}}[\eta_{uj}\Pi]-\sum_{i,j}\boldsymbol{d}_{ij}\frac{\partial}{\partial\eta_{vi}}[\eta_{vj}\Pi]\\ &-\sum_{i,j}\boldsymbol{f}_{ij}\frac{\partial}{\partial\eta_{vi}}[\epsilon_j\Pi]+\frac{1}{2}\sum_{i,j}\boldsymbol{\alpha}_{ij}\frac{\partial^2\Pi}{\partial\eta_{ui}\partial\eta_{uj}}+\sum_{i,j}\boldsymbol{\beta}_{ij}\frac{\partial^2\Pi}{\partial\eta_{ui}\partial\eta_{vj}}+\frac{1}{2}\sum_{i,j}\boldsymbol{\gamma}_{ij}\frac{\partial^2\Pi}{\partial\eta_{vi}\partial\eta_{vj}}+\frac{1}{2}\sum_{i,j}\boldsymbol{\delta}_{ij}\frac{\partial^2\Pi}{\partial\epsilon_i\partial\epsilon_j}.\end{aligned} \tag{23}$$

From this we can immediately derive the covariances as [22]

$$\langle \eta_{ul}\dot{\eta}_{um}\rangle = \sum_j \boldsymbol{a}_{lj}\langle \eta_{uj}\eta_{um}\rangle + \sum_j \boldsymbol{a}_{mj}\langle \eta_{ul}\eta_{uj}\rangle + \sum_j \boldsymbol{b}_{lj}\langle \eta_{vj}\eta_{um}\rangle + \sum_j \boldsymbol{b}_{mj}\langle \eta_{ul}\eta_{vj}\rangle + \sum_j \boldsymbol{e}_{lj}\langle \epsilon_j\eta_{um}\rangle + \sum_j \boldsymbol{e}_{mj}\langle \eta_{ul}\epsilon_j\rangle + \boldsymbol{\alpha}_{lm}, \tag{24}$$

$$\langle \eta_{ul}\dot{\eta}_{vm}\rangle = \sum_j \boldsymbol{a}_{lj}\langle \eta_{uj}\eta_{vm}\rangle + \sum_j \boldsymbol{b}_{lj}\langle \eta_{vj}\eta_{vm}\rangle + \sum_j \boldsymbol{c}_{mj}\langle \eta_{ul}\eta_{uj}\rangle + \sum_j \boldsymbol{d}_{mj}\langle \eta_{ul}\eta_{vj}\rangle + \sum_j \boldsymbol{e}_{lj}\langle \epsilon_j\eta_{vm}\rangle + \sum_j \boldsymbol{f}_{mj}\langle \eta_{ul}\epsilon_j\rangle + \boldsymbol{\beta}_{lm}, \tag{25}$$

$$\langle \eta_{vl}\dot{\eta}_{vm}\rangle = \sum_j \boldsymbol{c}_{lj}\langle \eta_{uj}\eta_{vm}\rangle + \sum_j \boldsymbol{c}_{mj}\langle \eta_{vl}\eta_{uj}\rangle + \sum_j \boldsymbol{d}_{lj}\langle \eta_{vj}\eta_{vm}\rangle + \sum_j \boldsymbol{d}_{mj}\langle \eta_{vl}\eta_{vj}\rangle + \sum_j \boldsymbol{f}_{lj}\langle \epsilon_j\eta_{vm}\rangle + \sum_j \boldsymbol{f}_{mj}\langle \eta_{vl}\epsilon_j\rangle + \boldsymbol{\gamma}_{lm}, \tag{26}$$

where $\dot{} = \partial/\partial t$ and $\langle ab\rangle$ denotes the covariance of a and b. Partial differential equations governing the covariances of $\langle \eta_{ul}\epsilon_m\rangle$, $\langle \epsilon_l\eta_{vm}\rangle$, and $\langle \epsilon_l\epsilon_m\rangle$ can be found similarly.

IV. SPATIAL FOURIER TRANSFORM

We now introduce the discrete spatial Fourier transform. We choose to use the discrete Fourier cosine expansion [14,25,46], since, by setting $k = m\pi/L$, $m = 0,1,\ldots,K-1$, we can incorporate the boundary terms as the cosine function naturally encapsulates the Neumann boundary conditions [28]. The transform has the explicit form

$$\widehat{f}(k) = \Delta_x \sum_{j=1}^{K} \cos[k\Delta_x(j-1)]f(x_j). \tag{27}$$

Note that the factor of $(j-1)$ in the cosine function is simply to correct for the fact that, spatially, we have defined our populations to start with an index one, instead of zero. Hence, the differential equations governing the spatial power spectrum of the system are specified by

$$\begin{aligned}\langle \widehat{\eta}_{uk}\dot{\widehat{\eta}}_{uk}\rangle &= [4a_1\cos(k\Delta_L) + 2a_0]\langle \widehat{\eta}_{uk}\widehat{\eta}_{uk}\rangle + 2b_0\langle \widehat{\eta}_{vk}\widehat{\eta}_{uk}\rangle \\ &\quad + [4e_1\cos(k\Delta_L) + 2e_0]\langle \widehat{\eta}_{uk}\widehat{\epsilon}_k\rangle \\ &\quad + \frac{\Delta_L^2 K}{2}(\alpha_0 + 2\cos(k\Delta_L)\alpha_1),\end{aligned} \tag{28}$$

$$\begin{aligned}\langle \widehat{\eta}_{uk}\dot{\widehat{\eta}}_{vk}\rangle &= [2(a_1+d_1)\cos(k\Delta_L) + a_0 + d_0]\langle \widehat{\eta}_{uk}\widehat{\eta}_{vk}\rangle \\ &\quad + b_0\langle \widehat{\eta}_{vk}\widehat{\eta}_{vk}\rangle + c_0\langle \widehat{\eta}_{uk}\widehat{\eta}_{uk}\rangle \\ &\quad + [2e_1\cos(k\Delta_L) + e_0]\langle \widehat{\epsilon}_k\widehat{\eta}_{vk}\rangle + [2f_1\cos(k\Delta_L) \\ &\quad + f_0]\langle \widehat{\eta}_{uk}\widehat{\epsilon}_k\rangle + \frac{\Delta_L^2 K}{2}\beta_0,\end{aligned} \tag{29}$$

$$\begin{aligned}\langle \widehat{\eta}_{vk}\dot{\widehat{\eta}}_{vk}\rangle &= [4d_1\cos(k\Delta_L) + 2d_0]\langle \widehat{\eta}_{vk}\widehat{\eta}_{vk}\rangle + 2c_0\langle \widehat{\eta}_{uk}\widehat{\eta}_{vk}\rangle \\ &\quad + [4f_1\cos(k\Delta_L) + 2f_0]\langle \widehat{\epsilon}_k\widehat{\eta}_{vk}\rangle \\ &\quad + \frac{\Delta_L^2 K}{2}(\gamma_0 + 2\cos(k\Delta_L)\gamma_1),\end{aligned} \tag{30}$$

where, for $w \in \{a,b,c,d,e,f,\alpha,\beta,\gamma,\delta\}$, w_0 and w_1 are the diagonal and off-diagonal elements of the submatrix $\boldsymbol{w}$, respectively. ODEs governing the Fourier transforms of the covariances for $\langle \widehat{\eta}_{uk}\widehat{\epsilon}_k\rangle$, $\langle \widehat{\epsilon}_k\widehat{\eta}_{vk}\rangle$, and $\langle \widehat{\epsilon}_k\widehat{\epsilon}_k\rangle$ can be found similarly. Hence, we have reduced the system from $6K \times 6K$ to six ODEs, which define the dynamics of the spatial power spectra of the stochastic variables. These equations tell us which spatial wave modes are activated and, thus, give us insights into the patterns we should expect. However, it should be noted that we have lost information concerning the cross correlations. This is not a problem, since we are only concerned with the activated wave modes predicted by the power spectra.

V. SIMULATION COMPARISON

We now face the problem of comparing theory with simulation. The derived theory is only applicable at the spatially homogeneous steady state. However, in the Turing unstable parameter region, the system will try to evolve into a patterned state, making the conclusions drawn from the theory invalid. Thus, we are in exactly the same situation as with deterministic Turing linear analysis; we can only predict to which modes a spatially uniform steady state is unstable and not which mode (or supposition of modes) will be finally displayed at steady state. Thus, the theory has two applications. First, it can be used to suggest which wave modes are being initially excited and question whether they correspond to the modes available in the deterministic system. Second, we can explore the parameter region outside the Turing unstable regime. In the deterministic regime we would obtain no patterns. However, it has been shown that, in this regime, the stochastic description of the problem may be able to support structures which have been referred to as "stochastic Turing patterns" [14,47].

A. Stationary domain

As an initial illustration, we simulate a deterministic system and compare it to its stochastic analog. To complement this, we investigate the stochastic and deterministic wave modes to which the uniform steady state is linearly unstable, both inside and outside of the deterministic Turing patterning parameter domain.

1. Inside the Turing parameter domain

Turing systems on stationary domains normally do not exhibit pattern selection robustness because the homogeneous steady state is generally unstable to multiple wave modes, as illustrated in Fig. 3. This figure shows that, as the length of the domain, L, increases, the number of possible final patterns

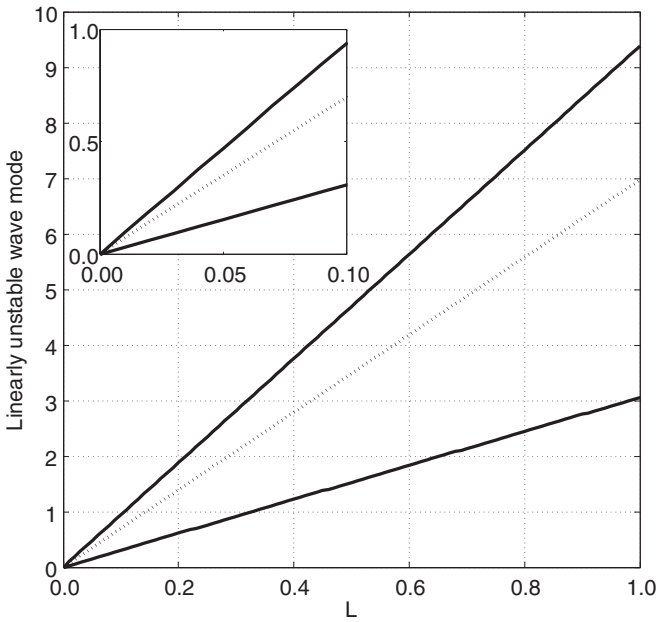

FIG. 3. Linearly growing wave modes of the Schnakenberg kinetics for varying domain lengths. The two solid lines delineate the region of possible linearly growing wave modes. The dotted line denotes the maximum eigenvalue of the dispersion relation, i.e., the fastest growing Fourier mode in the continuous system. The inset magnifies the region [0,0.1]. Parameters used: $D_u = 1 \times 10^{-4}$, $D_v = 1 \times 10^{-2}$, $\kappa_1 = 10$, $\kappa_3 = 0.2$, $\kappa_{-1} = 30$, and $\kappa_2 = 1 \times 10^{-5}$.

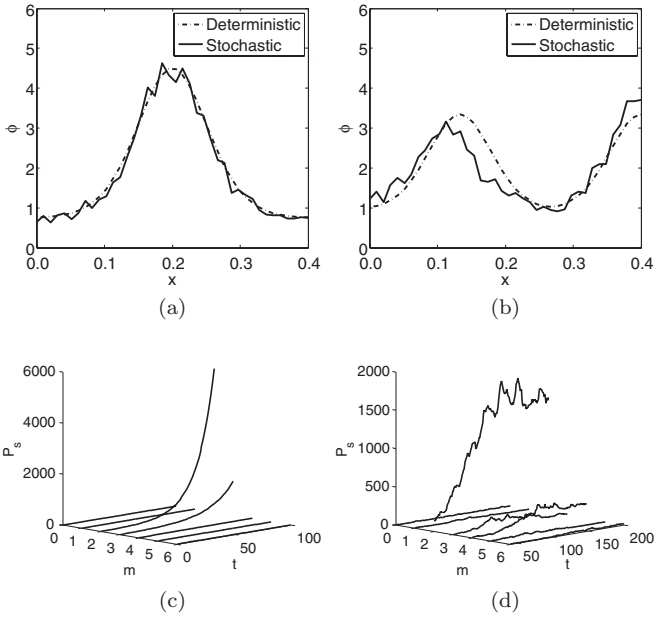

FIG. 4. (a, b) For the given parameter values, both wave mode two and three patterns are possible using the Schnakenberg kinetics (see the Appendix). Here we compare the stochastic and deterministic systems for each mode, respectively. (c) Evolution of the theoretical spatial power spectrum, Eq. (28), using the Schnakenberg kinetics. (d) Power spectrum of the single stochastic simulation shown in (a). Parameters used: $D_u = 1 \times 10^{-4}$, $D_v = 1 \times 10^{-2}$, $\kappa_1 = 10$, $\kappa_{-1} = 0.2$, $\kappa_2 = 30$ and $\kappa_3 = 1 \times 10^{-5}$, on a stationary domain of length $L = 0.4$ discretized into $K = 40$ compartments.

also increases. For example, when the length of the domain is $L = 0.4$, the spatially uniform steady state is unstable to wave modes two and three. Thus, from random initial conditions, we cannot be certain as to which final wave mode the system will evolve. However, similar to the case of deterministic Turing patterns, for small numbers of possible linearly growing wave modes we can expect that the fastest growing mode will generally dictate the solution of the system. Figures 4(a) and 4(b) show that modes two and three are realizable in both the stochastic and deterministic simulations.

By considering the spatial power spectra in Figs. 4(c) and 4(d), we can now compare the stochastically excited modes with the actual evolution of the system. Figure 4(c) clearly shows that both modes two and three are excited in the stochastic spectrum. The fact that wave mode two grows quicker than wave mode three offers a reason behind the difficulty in generating a mode-three wave pattern; out of 100 simulations, only seven displayed a stable mode-three pattern, similar to that shown in Fig. 4(b).

On comparing Figs. 4(c) and 4(d), we see that the theoretical power spectrum grows without limit, while the spectrum of the single stochastic realisation tends to a finite power value. This shows the limitation of the theory discussed at the start of Sec. V; i.e., since we are using a linearized version of the Fokker-Plank equation we can only predict the excited wave modes rather than their amplitude. This is comparable to the standard Turing analysis [10,35,48].

2. *Outside the Turing parameter domain*

To illustrate the second use of our theory, we now extend our investigation to parameter regions that do not allow deterministic systems to pattern. For $L = 0.1$, the inset of Fig. 3 suggests that no deterministic Turing patterns exist, which is confirmed by deterministic simulation (not shown). Contrarily, Fig. 5(a) clearly shows that the inclusion of noise promotes patterning. However, although stochastic Turing patterns are able to exist outside of the deterministic parameter domain, they are unable to stabilize over the entire simulation time. Due to the instability of these "stochastic Turing patterns," the structures are able to undergo polarity switching. Note that polarity switching is also possible within the normal Turing parameter region if noise levels are sufficiently high. However, it is realized more easily outside this region because of the competing effects that are occurring; the noise tends to pattern the domain, whereas the mean-field dynamics tend to homogenize the system.

In Fig. 5(c) we see that, since we are not inside the Turing unstable parameter region, the stochastically excited wave modes no longer continuously grow without bound and instead tend to a constant value of power. This compares well to the averaged power spectrum of the simulated data shown in Fig. 5(b). Here, we see the theory works far better than we would expect it to. As mentioned previously, we only expect a good comparison when the population is near its steady-state value, yet Fig. 5 clearly shows that the theory may hold even in situations where the stochastic kinetics are such that a spatial mode is being activated to move the system away from the steady state. Currently, there is a debate as to how the noise is able to act constructively over such long time scales. However, by considering Eqs. (28)–(30), we can be sure that the wave

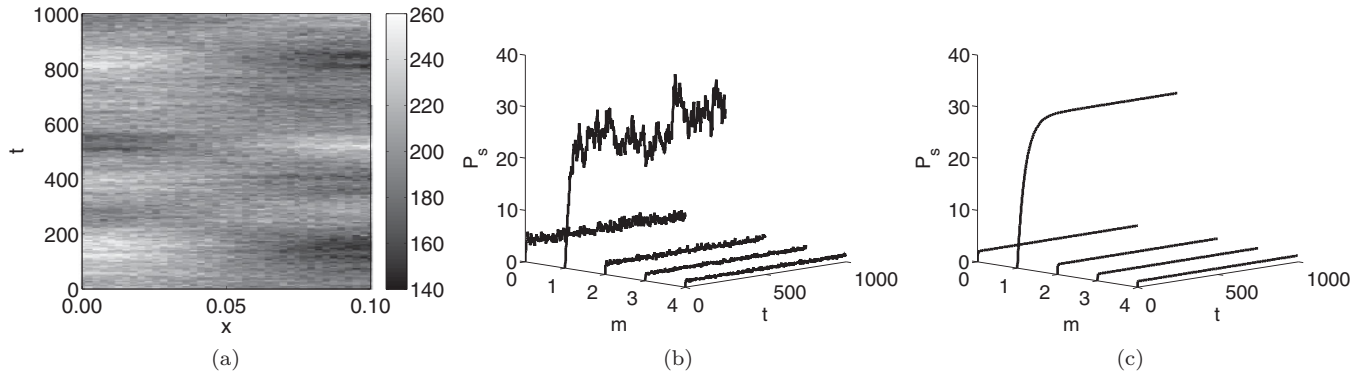

FIG. 5. (a) Evolution of the population U during a single stochastic simulation with Schnakenberg kinetics. (b) Averaged power spectrum of 100 simulations. (c) Evolution of the theoretical spatial power spectrum, Eq. (28), with Schnakenberg kinetics (see the Appendix). Parameters used: $D_u = 1 \times 10^{-4}$, $D_v = 1 \times 10^{-2}$, $\kappa_1 = 10$, $\kappa_{-1} = 0.2$, $\kappa_2 = 30$, $\kappa_3 = 1 \times 10^{-5}$, and $\Omega = 100$ on a stationary domain of length $L = 0.1$ discretized into $K = 40$ compartments. For the given parameters the steady state is $U = 200$.

modes are excited due to the second-order moments of our Gaussian approximation to the noise.

B. Comparing deterministic and stochastic growth

Having seen that the intrinsic noise of reactions can affect the patterning properties of a Turing system on a stationary domain, we now include growth to see how this influences mode selection.

In Fig. 6 we compare not only the deterministic evolution of Schnakenberg kinetics to their stochastic analogues but we also illustrate the difference between stochastic and deterministic descriptions of growth. Starting from an initial length of $L = 0.4$ the domain was allowed to grow uniformly linearly as $n = 1 + rt/\theta$ at a rate of $r/\theta = 1 \times 10^{-4}$. Thus after 10^4 time steps the domain doubles in size, to $L = 0.8$. By considering Fig. 3 we can see that, for a domain of length $L = 0.4$, the system can evolve to a final pattern of wave mode two or three, whereas when the length of the domain is $L = 0.8$, the system can evolve to a final pattern of any integer wave mode between three and seven, inclusive. This evolution of activated modes is captured in Figs. 6(d) and 6(e) where, initially, mode two has the highest power but as time increases further wave modes are activated. As the simulation reaches $t = 2220$ the growth of the second mode begins to slow down and eventually reduces, whilst the third mode overtakes it as the most strongly excited mode. This transition can be linked to the breakdown of period doubling that occurs in the transition from deterministic kinetics to stochastic kinetics, as seen in Figs. 6(a)–6(c), although the realization of the transition occurs much later in the simulated system than estimated from the covariance ODEs.

From comparing Figs. 6(b), 6(c), 6(d), and 6(e) we can conclude that the inherent noise of the reactions far outweighs the noise generated from the stochastic description of growth, since qualitatively the figures are the same. However, it should be noted that the stochastic growth spectrum has a higher power. The only noticeable difference in the simulations being that, as expected, the stochastic growing domain simulation is noisier; the maximum range of the solution is larger than the deterministic growth simulation and the transition from mode two to three occurs earlier. Practically, this implies that it is sufficient to consider deterministic growth.

In both the situations of growing and static domains, whenever we are inside the Turing unstable parameter region the noise excites the same modes as the deterministic Turing analysis. Particularly, due to consecutive wave mode excitation, the primary effect of growth is seen to remove peak-splitting as the mechanism of transition and replace it with consecutive increasing of the wave mode of the solution. This correspondence of activated wave modes is proved in Sec. VI.

C. Mechanisms of robustness

In the previous section we saw that stochasticity caused a breakdown of robustness via mode doubling. Although this loss of robustness may not be surprising, it does lead us to question the sensitivity of the pattern doubling mechanism, i.e., will arbitrarily small noise lead to a breakdown of pattern doubling? Furthermore, is this new mechanism of consecutive mode excitation robust?

Theoretically, as the population scale, Ω, becomes larger, the stochastic simulations should approximate their deterministic counterparts better. The effect of increasing Ω can be seen in Fig. 7, where, for values of $\Omega \leqslant 10^4$, the pattern doubling mechanism breaks down as the system undergoes the transition from wave mode two to three. Although $\Omega = 10^4$ is nowhere near the number of molecules in a mole (10^{23}), numerically we are at the limit of our computational power using single particle interactions. Thus, to consider stochastic effects within larger populations, we use a Langevin framework in which the noise is correctly scaled (Fig. 8) [49–51]. Although this is only an approximation of the system under consideration, as we have moved from a discrete case description to a continuous description, it will at least suggest if the transitions are stable against any form of noise, or whether stochasticity singularly perturbs the deterministic system. From Fig. 8 we see the first signs of robust doubling reappearing, as the transition $2 \mapsto 4$ stabilizes for $\Omega \geqslant 10^6$ and, further, the transition $2 \mapsto 4 \mapsto 8$ is observed in Fig. 8(b). Thus, we conjecture that as the

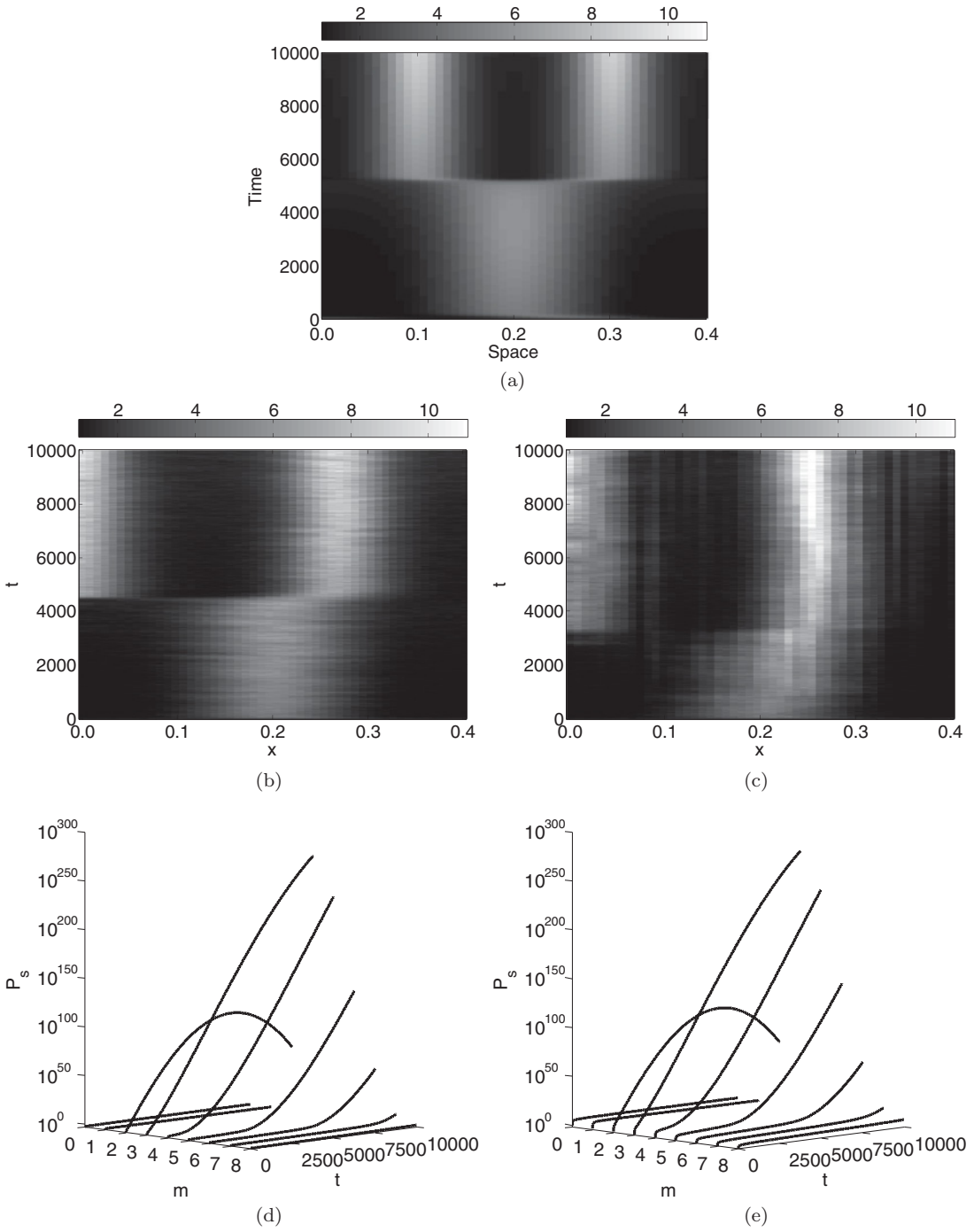

FIG. 6. (a) Deterministic evolution of the Schnakenberg equations on a linearly growing domain. (b) Stochastic Schnakenberg kinetics on a deterministically, linearly growing domain. (c) Stochastic Schnakenberg kinetics on a stochastically, linearly growing domain. (d, e) Evolution of the corresponding theoretical power spectra, $\langle \widehat{\eta}_{uk} \widehat{\eta}_{uk} \rangle$, on deterministically and stochastically growing domains, respectively. Note that the plots have a log scale. Parameters used: $D_u = 1 \times 10^{-4}$, $D_v = 1 \times 10^{-2}$, $\kappa_1 = 10$, $\kappa_{-1} = 0.2$, $\kappa_2 = 30$, $\kappa_3 = 1 \times 10^{-5}$, $\Omega = 100$, $\theta = 100$, and $r/\theta = 10^{-4}$. The initial length of the domain is $L = 0.4$ and there are $K = 50$ compartments.

parameter Ω increases, the doubling transitions will become more and more common. However, for any finite value of Ω there will come a time point at which the stochastic transitions diverge from the deterministic transitions. This is because, as the system evolves to higher and higher wave modes, the bifurcation diagram increases in complexity and therefore it is more likely that the simulations will exhibit one of the other possible modes [32]. This breakdown of period doubling is also compounded by the fact that we are using linearly growing domains, as it has been shown analytically that only exponentially growing domains can support period doubling in the deterministic case. Hence, for all subexponential growth rates, there will come a point at which even the deterministic system is unable to maintain a pattern doubling transition.

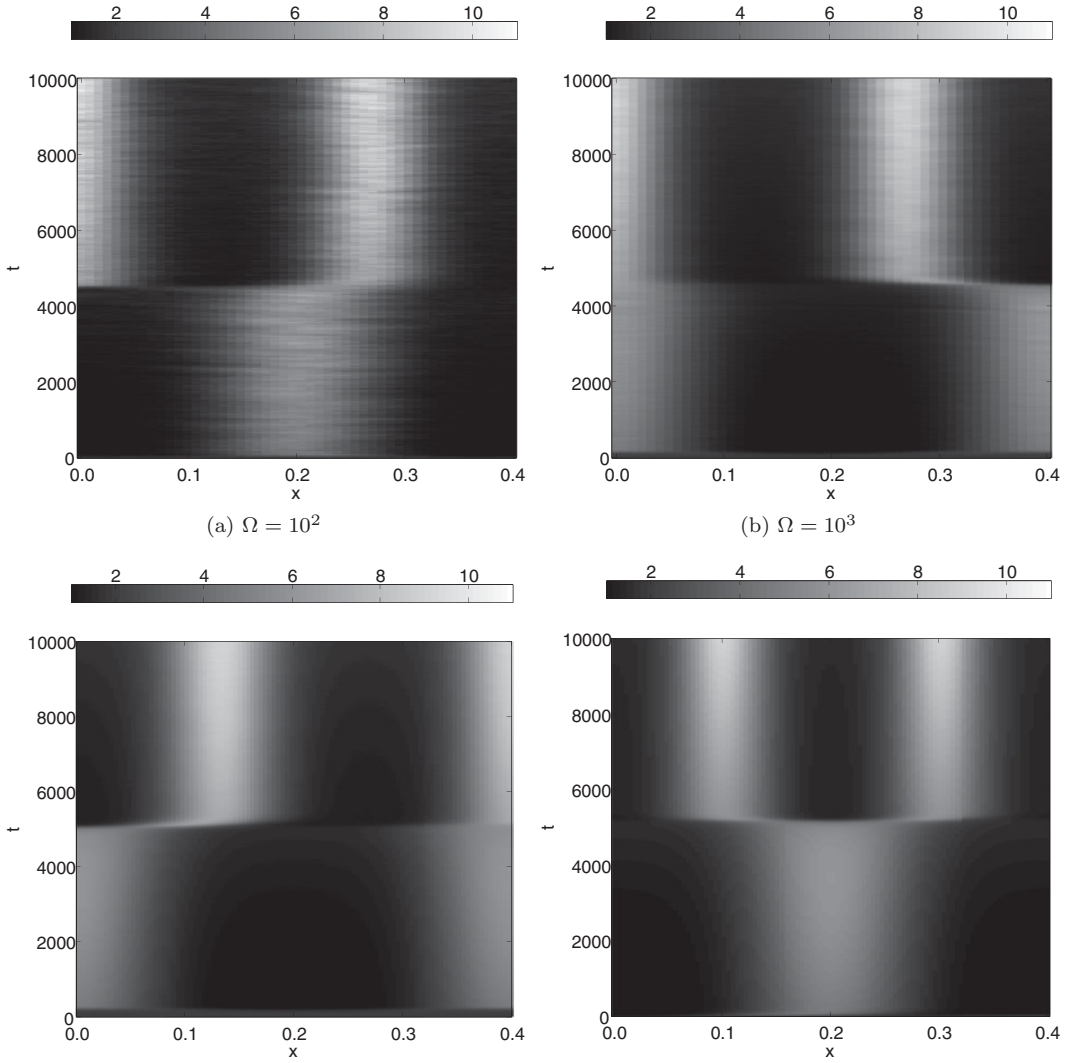

(a) $\Omega = 10^2$ (b) $\Omega = 10^3$

(c) $\Omega = 10^4$ (d) Deterministic simulation

FIG. 7. Stochastic simulations with increasing value of Ω, noted beneath each figure. Parameters are $D_u = 1 \times 10^{-4}$, $D_v = 1 \times 10^{-2}$, $\kappa_1 = 10$, $\kappa_{-1} = 0.2$, $\kappa_2 = 30$, $\kappa_3 = 1 \times 10^{-5}$, and $r/\theta = 10^{-4}$. Initially the length of the domain was $L = 0.4$ and the domains in (a) and (b) were discretized into $K = 50$ compartments, whereas the domains in (c) and (d) were discretized into $K = 100$ boxes.

Since our primary concern is with low copy number systems, we must return to the hypothesis that, although pattern doubling is not robust, it may be possible to use consecutive wave number increase as a mechanism of robustness, as suggested by Fig. 6. In Fig. 9 we show the results of repeated simulation of the stochastic system for cases with $K = 50$ Lagrangian boxes (top row) and $K = 100$ Lagrangian boxes (bottom row) to demonstrate that the domain discretization was not affecting the simulations. The simulations show that the phenomenon of sequentially increasing wave numbers is not completely robust as, although the majority of simulations do show transitions $2 \mapsto 3 \mapsto 4$, after this transitions $4 \mapsto 5$ and $4 \mapsto 6$ are both seen and, furthermore, the transition $2 \mapsto 4$ is also possible. Also note that we have no control over the polarity of the solution. Thus, we conclude that, for systems that contain only a small number of active particles, uniformly growing domains may be able to support robust sequences of the lower wave modes. For further evidence of this claim, see Fig. 10. Here, we have simulated the evolution of 100 stochastic systems and calculated the dominant wave mode at each time point. Clearly we see that the most likely transition sequence is a consecutively increasing one, since the wave mode with the highest probability increases consecutively. However, this probability reduces with increasing number of active wave modes. For example, the probability that the system will exhibit a wave mode two pattern during the first 5000 time units is 0.98. Similarly, the probability the system will exhibit a mode three pattern during the next 5000 time units is 0.96. Interestingly, although we can see that the probability of being in a particular state decreases over time, due to more wave modes becoming available, this decrease is not monotonic. Indeed, over the regions where the probability of being in an even mode is highest, this probability is higher than the probability of the preceding odd mode. For example, the probability of being in a mode six pattern during $t \approx 25000-30000$ time units is 0.87, whereas the probability

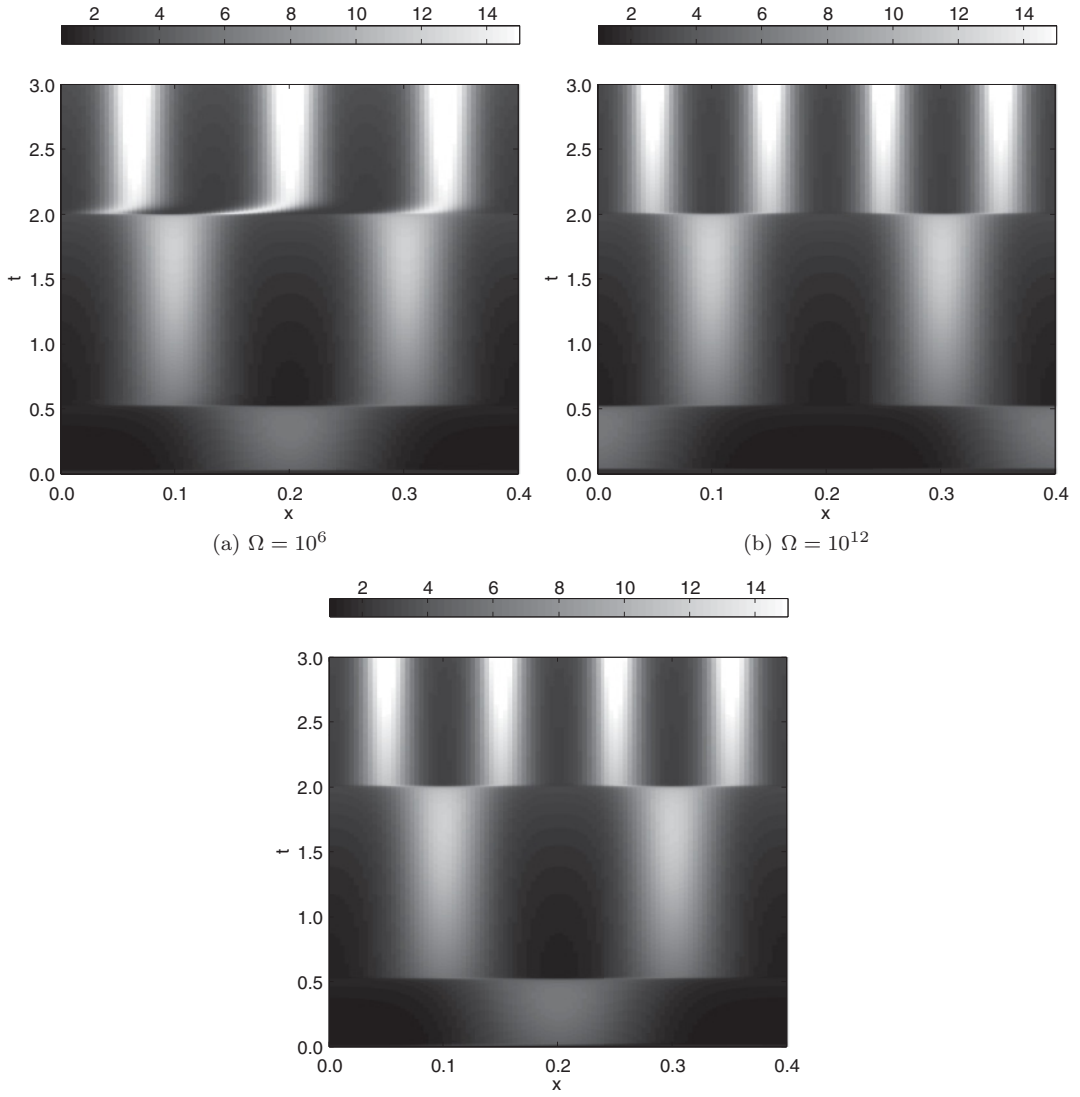

(a) $\Omega = 10^6$

(b) $\Omega = 10^{12}$

(c) Deterministic simulation

FIG. 8. Langevin simulations with increasing value of Ω, noted beneath each figure. Parameters are $D_u = 1 \times 10^{-4}$, $D_v = 1 \times 10^{-2}$, $\kappa_1 = 10, \kappa_{-1} = 0.2, \kappa_2 = 30, \kappa_3 = 1 \times 10^{-5}$, and $r/\theta = 10^{-4}$. Initially the length of the domain was $L = 0.4$ and the domains were discretized into $K = 100$ boxes.

of being in a mode five pattern during $t \approx 20000-25000$ is 0.81. This can be explained by reasoning that it is an artefact of the mean-field causing the system to exhibit mode-doubling. Hence, although small transition sequences of consecutive increasing modes are likely, they are not certain. This was also commented upon by Arcuri and Murray [52], who studied deterministic Turing systems on growing domains. They incorporated growth through a simple scaling argument rather than a derivation from first principles, and noticed that their systems would often miss certain wave modes during their evolution. Hence, they concluded that patterns must form sequentially as any mechanism that acts over the whole domain is subject to too many sources of error to be capable of robust pattern formation at high wave modes. Although they did not include a dilution term, which we can now account for if the growth is isotropic, in the stochastic setting we are unable to generate robustness successfully on uniformly growing domains.

VI. ANALYSIS OF THE COVARIANCE ODES

Simulations seem to suggest that, inside the parameter region that realizes deterministic Turing patterns, the excited wave modes of the stochastic Schnakenberg system correspond to its deterministic analog, although the transition sequences may not. From considering a general reaction-diffusion system on a deterministic, uniformly growing domain that has been mapped onto a Lagrangian domain,

$$\frac{\partial \phi}{\partial t} = \frac{D_u}{n^2}\frac{\partial^2 \phi}{\partial x^2} + f(\phi,\psi,t), \tag{31}$$

$$\frac{\partial \psi}{\partial t} = \frac{D_v}{n^2}\frac{\partial^2 \psi}{\partial x^2} + g(\phi,\psi,t), \tag{32}$$

we intend to show that this is true for all Turing systems. As we are assuming slow growth, we use a quasi-steady-state hypothesis and, thus, fix $n = 1$.

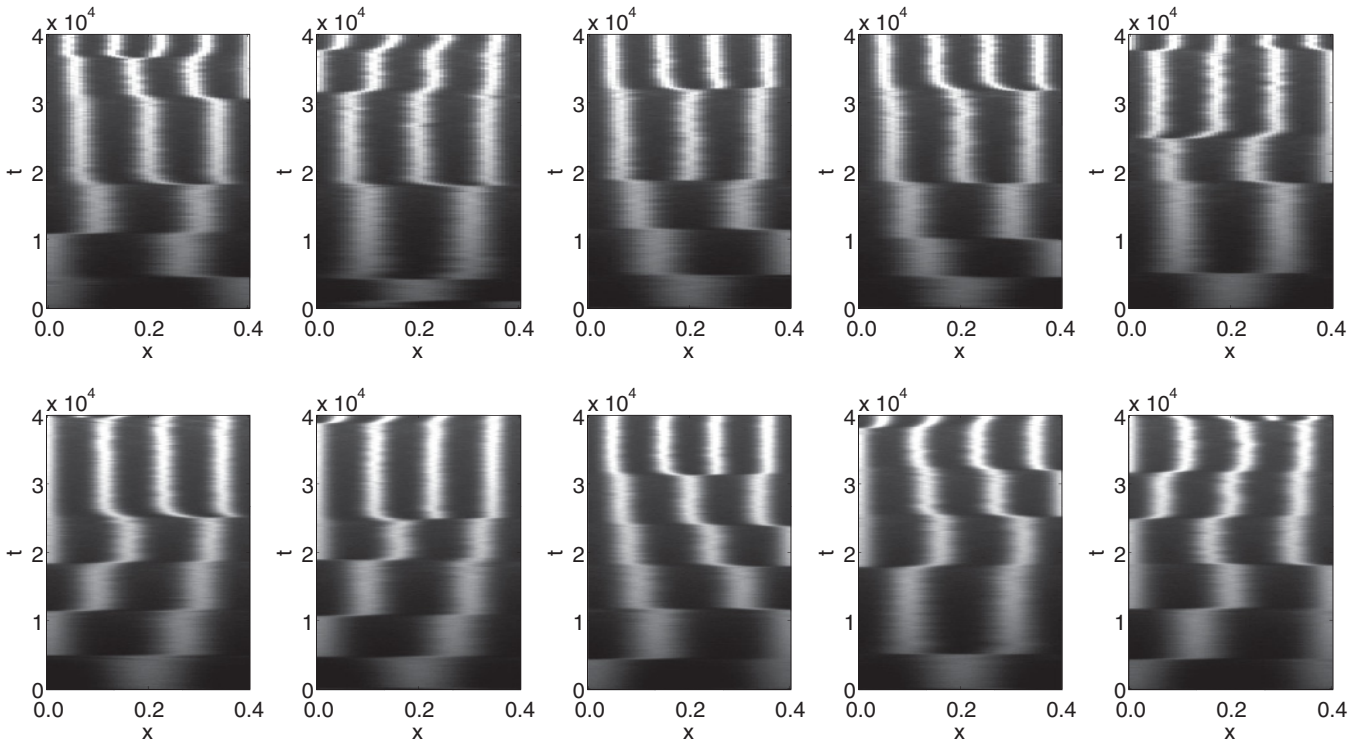

FIG. 9. Ten stochastic simulations with varying numbers of Lagrangian boxes. Top row: $K = 50$. Bottom row: $K = 100$. Parameters $D_u = 1 \times 10^{-4}$, $D_v = 1 \times 10^{-2}$, $\kappa_1 = 10$, $\kappa_{-1} = 0.2$, $\kappa_2 = 30$, $\kappa_3 = 1 \times 10^{-5}$, $\Omega = 100$, $\theta = 100$, and $r/\theta = 10^{-4}$. Initial length of domain $L = 0.4$. The color map is from 0 (black) to 20 (white).

From the reaction system that produces the kinetic functional forms f and g, we can derive the propensity functions and stoichiometric matrix (see the Appendix). Then, using Eqs. (7) and (8), we can calculate the matrices $\boldsymbol{A}$ and $\boldsymbol{B}$ from the definitions in Eqs. (11) and (12), which allows us to construct the ODE system of Fourier-transformed covariances in Eqs. (28)–(30). Rewriting this as a matrix ODE equation we obtain

$$\dot{\boldsymbol{X}} = \boldsymbol{M}\boldsymbol{X} - \boldsymbol{V}, \tag{33}$$

where $\boldsymbol{X}^T = [\langle\widehat{\eta}_{uk}\widehat{\eta}_{uk}\rangle, \langle\widehat{\eta}_{uk}\widehat{\eta}_{vk}\rangle, \langle\widehat{\eta}_{vk}\widehat{\eta}_{vk}\rangle]$, the explicit form of $\boldsymbol{M}$ is

$$\boldsymbol{M} = \begin{bmatrix} 4\,a_1\,\cos(k\Delta_L) + 2\,a_0 & 2\,b_0 & 0 \\ c_0 & 2\,a_1\,\cos(k\Delta_l) + a_0 + 2\,d_1\,\cos(k\Delta_l) + d_0 & b_0 \\ 0 & 2\,c_0 & 4\,d_1\,\cos(k\Delta_L) + 2\,d_0 \end{bmatrix}, \tag{34}$$

and $\boldsymbol{V}$ is defined appropriately from Eqs. (28)–(30). Since Eq. (33) is linear and autonomous, we can solve the ODEs analytically yielding a solution that is the linear sum of three exponential functions with exponents

$$\lambda_1 = 2a_1\cos(k\Delta_L) + a_0 + 2d_1\cos(k\Delta_L) + d_0, \tag{35}$$

$$\begin{aligned}\lambda_\pm = {} & 2a_1\cos(k\Delta_L) + a_0 + 2d_1\cos(k\Delta_L) + d_0 \\ & \pm[4(a_1 - d_1)^2(\cos(k\Delta_L) - 1)^2 \\ & + 4(a_1 - d_1)(2a_1 + a_0 - d_0 - 2d_1)\cos(k\Delta_L) \\ & + (a_0 - d_0)^2 - 4(d_1 - a_1)^2 + 4b_0c_0]^{\frac{1}{2}}.\end{aligned} \tag{36}$$

The existence of such a solution also depends on these three values not being zero, which is always satisfied inside the Turing domain, as shown below.

Since we are only interested in the coefficients matrix, $\boldsymbol{M}$, of the Fourier-transformed covariances, we only need to consider the matrix $\boldsymbol{A}$. This can be split up into four $K \times K$ submatrices,

$$\mathbf{A} = \begin{bmatrix} \boldsymbol{a} & \boldsymbol{b} \\ \boldsymbol{c} & \boldsymbol{d} \end{bmatrix}, \tag{37}$$

where $\boldsymbol{a}$ and $\boldsymbol{d}$ are symmetric and tridiagonal and $\boldsymbol{b}$ and $\boldsymbol{c}$ are diagonal. From their definitions Eq. (11) we can show that $\boldsymbol{b} = \partial f/\partial\psi\,\boldsymbol{I} = b_0\boldsymbol{I}$ and $\boldsymbol{c} = \partial g/\partial\phi\boldsymbol{I} = c_0\boldsymbol{I}$, where $\boldsymbol{I}$ is the

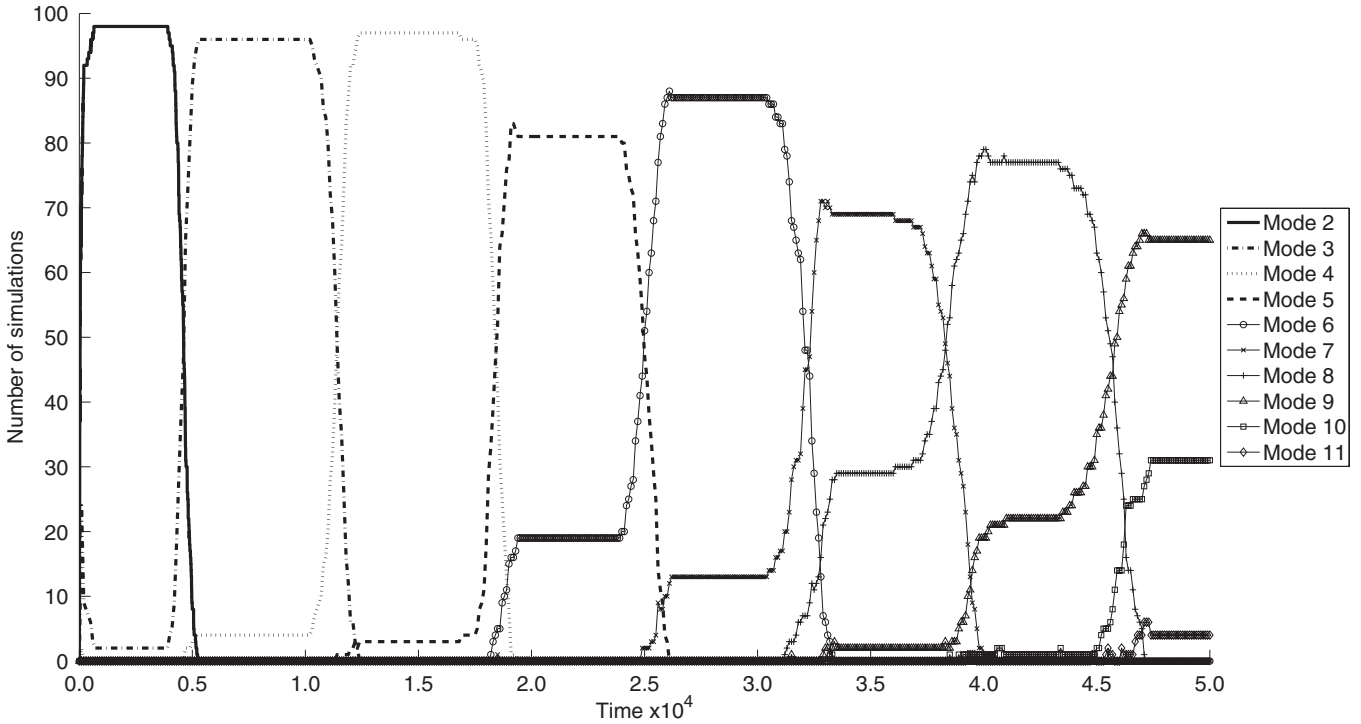

FIG. 10. Exhibited wave modes of 100 simulations using the same parameters as described in the legend of Fig. 9. The domain was discretized into 100 Lagrangian compartments.

$K \times K$ identity matrix. The diagonal and off-diagonal values of $\boldsymbol{a}$ are

$$a_0 = \frac{-2D_u K^2}{L^2} + \frac{\partial f}{\partial \phi}, \tag{38}$$

$$a_1 = \frac{D_u K^2}{L^2}, \tag{39}$$

respectively, whereas

$$d_0 = \frac{-2D_v K^2}{L^2} + \frac{\partial g}{\partial \psi}, \tag{40}$$

$$d_1 = \frac{D_v K^2}{L^2}, \tag{41}$$

are the diagonal and off-diagonal elements, respectively, of $\boldsymbol{d}$. Each term is evaluated at the homogeneous steady state, $\phi_i = \phi^*$ and $\psi_i = \psi^*$, for all values of i.

Substituting these values into Eqs. (35) and (36), we obtain

$$\lambda_1 = 2\frac{D_u K^2}{L^2}[\cos(k\Delta_L) - 1] + 2\frac{D_v K^2}{L^2}[\cos(k\Delta_L) - 1] + f_\phi + g_\psi, \tag{42}$$

$$\lambda_\pm = \lambda_1 \pm \left\{ 4\left[\frac{D_u K^2}{L^2} - \frac{D_v K^2}{L^2}\right]^2 [\cos(k\Delta_L) - 1]^2 + 4(f_\phi - g_\psi)\left[\frac{D_u K^2}{L^2} - \frac{D_v K^2}{L^2}\right][\cos(k\Delta_L) - 1] + 4(g_\phi f_\psi - f_\phi g_\psi) + (f_\phi + g_\psi)^2 \right\}^{\frac{1}{2}}. \tag{43}$$

Since $[\cos(k\Delta_L) - 1] \leqslant 0$ and inside the Turing region we know that $f_\phi + g_\psi < 0$ [48], it follows that λ_1 and $\mathrm{Re}(\lambda_-)$ are negative. Hence, the only way to obtain an excited mode in the Turing region is if $\mathrm{Re}(\lambda_+) > 0$. In order to satisfy this condition the following inequality for $y = [\cos(k\Delta_L) - 1]$ must be satisfied:

$$\frac{4D_u D_v K^4}{L^4} y^2 + \frac{2K^2}{L^2}(f_\phi D_v + D_u g_\psi) y + f_\phi g_\psi - g_\phi f_\psi < 0. \tag{44}$$

Thus, excited modes will exist for

$$-\frac{L^2}{K^2} y_+ < y < -\frac{L^2}{K^2} y_-, \tag{45}$$

where

$$y_\pm = \frac{f_\phi D_\psi + g_\psi D_\phi \pm \sqrt{(f_\phi D_\psi + D_\phi g_\psi)^2 - 4D_\phi D_\psi (f_\phi g_\psi - f_\psi g_\phi)}}{4D_\phi D_\psi}. \tag{46}$$

Note that inside the Turing unstable domain $y_\pm$ are real and so the steady state is unstable whenever

$$1 - \frac{L^2}{K^2} y_+ < \cos(k\Delta_L) < 1 - \frac{L^2}{K^2} y_-. \tag{47}$$

Thus, whenever the two limits of this range are within $[-1,1]$ we can invert the cosine function to obtain:

$$\frac{\arccos\left(1 - y_- \frac{L^2}{K^2}\right)}{\Delta_L} < k < \frac{\arccos\left(1 - y_+ \frac{L^2}{K^2}\right)}{\Delta_L}. \tag{48}$$

Since K is the number of compartments then to make sure the domain discretization does not interfere with the simulations we make K large and, hence, we are able to expand the arccos operator in terms of large K:

$$\sqrt{2y_-}\left[1 + \frac{1}{12} y_- \left(\frac{L}{K}\right)^2\right] \lesssim k \lesssim \sqrt{2y_+}\left[1 + \frac{1}{12} y_+ \left(\frac{L}{K}\right)^2\right]. \tag{49}$$

Letting $K \to \infty$, or $\Delta_L \to 0$, in such a way that $L = K\Delta_L$ remains constant, space becomes a continuum and, thus, using $k = m\pi/L$,

$$\frac{\sqrt{2y_-}}{\pi} L = m_- < m_c < m_+ = \frac{\sqrt{2y_+}}{\pi} L. \tag{50}$$

Using Eq. (46), inequality Eq. (50) can be compared exactly with the activated modes derived from the deterministic Turing analysis [48]. Hence, we can see that inside the deterministically unstable Turing parameter region, the stochastically excited modes are exactly the same as the Turing excited modes.

However, this is only true in the limit $K \to \infty$. In a discretized domain of K boxes there can be, at most, K active wave modes and, as the domain grows, higher wave modes also have the possibility of growing. As the activated wave modes tend to the number of boxes, the noise is able to excite higher wave modes than otherwise expected. For example, consider the dotted line in Fig. 11. This shows the stochastically excited modes when the domain is discretized into 25 boxes. As the number of modes increases, the line begins to distort until its tangent becomes infinite at wave mode 25. In terms of inequality Eq. (47), the lower root has reduced to below -1, implying that the equation no longer has two, real solutions.

For a given length, L, we are able to use the upper boundary of inequality Eq. (49) to define a lower bound on K,

$$\begin{aligned} m &= \frac{kL}{\pi}, \\ &\approx \frac{L}{\pi}\sqrt{2y_+}\left[1 + \frac{1}{12} y_+ \left(\frac{L}{K}\right)^2\right], \\ &= m_+ + \frac{\sqrt{2}}{12\pi} y_+^{3/2}\left(\frac{L^3}{K^2}\right). \end{aligned} \tag{51}$$

The discretization of the space will become inadequate when it allows higher wave modes to be amplified than would be expected by the deterministic Turing analysis. From Eq. (51), we see that we need to choose K satisfying

$$\frac{\sqrt{2}}{12\pi} y_+^{\frac{3}{2}} \frac{L^3}{K^2} < 1, \quad \Rightarrow \frac{y_+^{\frac{3}{4}} L^{\frac{3}{2}}}{\sqrt{6\sqrt{2}\pi}} < K. \tag{52}$$

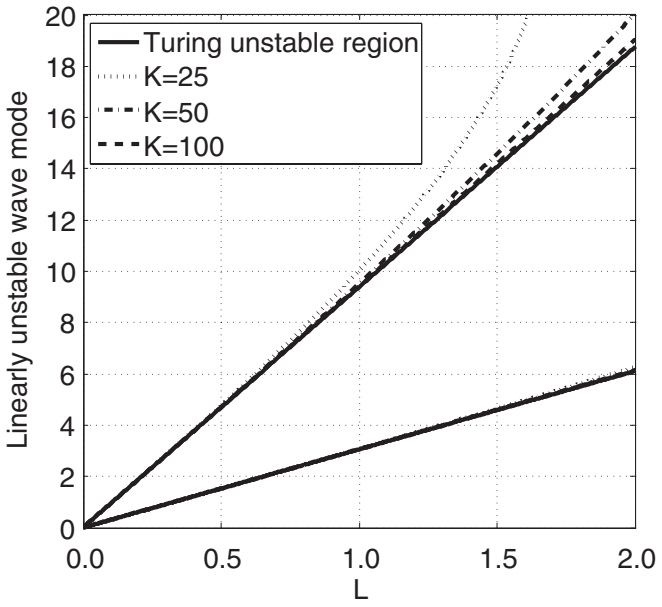

FIG. 11. Comparison of linearly growing wave modes of the deterministic Turing analysis (black solid lines) and noise-excited wave modes for different numbers of boxes, K, using the upper and lower bounds of inequalities Eqs. (47) and (50). Parameters are $D_u = 1 \times 10^{-4}$, $D_v = 1 \times 10^{-2}$, $\kappa_1 = 10$, $\kappa_{-1} = 0.2$, $\kappa_2 = 30$ and $\kappa_3 = 1 \times 10^{-5}$. Note that the lines delineating the lower bounds all lie approximately on top of each other.

Inequality Eq. (52) suggests that the number of boxes in the discretized system needs to grow faster than the length due to the exponent of $3/2$. For the small-scale systems we are simulating, we can easily choose K large enough not to violate this condition. However, for larger values of L we would need a much larger value of K and thus a much finer discretization. Since our analysis uses the weak-noise limit, this would mean including a larger number of simulated particles. This combination of factors implies that as the domain becomes larger the Gillespie SSA will take longer to simulate the system, as each time step becomes smaller due to the propensities increasing with the number of particles.

VII. CONCLUSION

In this work we have applied previously developed Fourier transform techniques to Turing reaction-diffusion systems on growing domains [28,29]. Our aim was to consider the lack of robustness that is apparent in such paradigm models, when the uniform steady state is linearly unstable to multiple wave modes [53]. It has been shown in the deterministic case that, upon placing Turing systems on uniformly growing domains, robust peak doubling sequences can be generated [30]. However, upon stochastically simulating the systems we have found that this robustness is lost.

First, we considered the specific example of the Schnakenberg kinetics on a stationary domain. Here it was seen that, within the deterministic Turing instability regime, the uniform steady state of the stochastic system is linearly unstable to exactly the same wave modes as the deterministic system.

However, although we were able to suggest which wave modes were excited, we were unable to predict which mode the final pattern would adopt. This is similar to the standard Turing analysis, which, due to the linearization process, suggests that all excited modes tend to grow exponentially and ignores higher-order terms that become important as the solution evolves. In the stochastic case, due to our use of a linear noise expansion, we also lose the higher-order effects and, thus, our analysis is only valid around the homogeneous steady state.

Although we are unable to predict exactly to which mode the system is going to evolve, if the number of excited modes is small then the power spectrum suggests which mode grows most quickly. This, in turn, suggests to which mode the system will tend. This was demonstrated in Fig. 4, where the power spectrum suggests that both modes two and three are excited, although wave mode two grows more quickly. This correlates with the fact that, out of 100 stochastic simulations, 93 yielded a stable mode two pattern, whereas only seven exhibited a stable wave mode three pattern. This correlation between highest power mode and realized stable pattern was also seen in the growing domain simulations (Fig. 6). Here, the power spectrum shows that, although wave mode two is initially the highest power mode, during growth wave mode three surpasses mode two to become the dominant mode. This can then be linked to the exact same transition in the simulated systems.

Parameters outside the deterministic Turing unstable region were then considered. Although such stochastic Turing patterns have been noted before [14], our simulations are, to our knowledge, the first numerical evidence of their actual existence. Further, we have discovered that, due to stochastic effects, polarity switching is possible (Fig. 5). Due to the systems lying outside the deterministic patterning parameter region, the activated modes no longer grow exponentially and we see a good comparison between the theoretical and simulated power spectra. Since the theory only holds near the homogeneous steady state and noise forces the system away from this state, this excellent correspondence is quite unexpected. As we move away from the deterministic Turing parameter region, the patterns become less pronounced, until it is difficult to observe patterns at all. Thus, since we are unable to clearly predict how much noise is needed to create a pattern, we simply focus on calculating the activated wave modes within the deterministically derived Turing domain.

Having investigated the stationary domain, we then moved on to consider uniformly growing domains. Immediately, it was seen that stochastic effects destroy any hope of robust peak doubling sequences when population numbers are low. By comparing stochastic and deterministic growth, we see that the noise generated by reactions is more important than the noise generated by stochastic domain growth. Indeed, it is due to the kinetics that activated modes grow exponentially, the effect of stochastic domain growth is simply to increase the power of all modes.

Using this knowledge we focused simply on deterministic growth, which further reduced the system of Fourier covariance ODEs. Using general reaction-diffusion equations we were able to show that the stochastic Turing modes were able to grow exponentially and, further, that these excited modes exactly correspond to their analogous deterministic Turing modes. This has allowed us to suggest that the reason that the peak doubling sequences break down is that the simulations simply switch to the highest power mode, which increases consecutively.

In Sec. V C we investigated this breakdown further and questioned whether stochasticity was a singular perturbation of the deterministic system. Since the noise scales as $1/\sqrt{\Omega}$, we increased Ω to our computational limit and saw that for sufficiently large populations, $\Omega = 10^6 - 10^{12}$, period doubling can be realized, at least for the first couple of transitions. If we now compare these particle numbers to a physical system of Turing patterns over a single cell [54], we see that a Dictyostelium cell has a volume of order $10^{-16}\,\mathrm{m}^3$ and, thus, it could contain on the order of 10^7 particles. As seen in Fig. 8(a), by this point the stochastic effects in the system are incredibly small. Hence, systems of this size and larger could be justified to act as a continuum. However, there are many biological systems that depend on very low copy numbers of active proteins, e.g., the genome of the bacterium *Escherichia coli*, where there are only 10–30 molecules of the lac repressor, which is involved in the regulation of gene expression [55]. Thus, our focus on small population numbers is fully justified.

Furthermore, in this low copy number regime, even the consecutive inclusion of wave modes is not robust on uniformly growing domains when the homogeneous steady state is unstable to large numbers of wave modes. In this case, predicting the evolution of the pattern is incredibly difficult. Thus, our results support those of Arcuri and Murray [52], who concluded that patterns must form sequentially as any mechanism that acts over the whole domain is subject to too many sources of error to be capable of robust pattern formation at high wave modes. Hence, to generate robustness, in a stochastic environment, we suggest apical growth as a plausible mechanism that can robustly support consecutive wave mode increasing pattern sequences (see Fig. 12). Thus, if apical domain growth and wave number were connected in some form of feedback loop then, once the desired wave

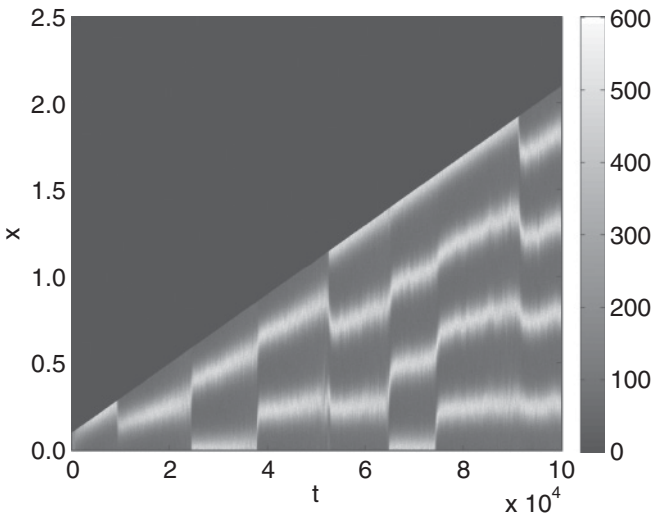

FIG. 12. Stochastic Schnakenberg kinetics simulated on a deterministic apically growing domain. Parameters are $D_u = 1 \times 10^{-4}$, $D_v = 1 \times 10^{-2}$, $\kappa_1 = 10$, $\kappa_{-1} = 0.2$, $\kappa_2 = 30$, $\kappa_3 = 1 \times 10^{-5}$, $\Omega = 100$, and $r/\theta = 1/5 \times 10^3$. Initially, $L = 0.1$ and the domain was discretized into 25 boxes.

number is reached, growth would stop, leaving a stable pattern of exactly the desired wave mode.

ACKNOWLEDGMENTS

T.E.W. thanks the EPSRC for support. P.K.M. was partially supported by a Royal Society-Wolfson Research Merit Award.

APPENDIX: SCHNAKENBERG EXAMPLE

Letting κ_i be the stochastic rate of reaction, the Schnakenberg system [56,57] consists of the chemical reactions

$$\emptyset \xrightarrow{\kappa_1} U, \quad U \xrightarrow{\kappa_{-1}} \emptyset, \quad \emptyset \xrightarrow{\kappa_2} V, \quad 2U + V \xrightarrow{\kappa_3} 3U, \tag{A1}$$

plus diffusion of the two reacting species. We consider the Schnakenberg system on a uniformly growing domain, which causes the Eulerian coordinates, x_E, to behave like $x_E = x_L n(t)$, where x_L is the fixed Lagrangian coordinate and $n(t)$ encapsulates the definition of growth [noting $n(0) = 1$]. The mean-field equations take the form [30,43,44]

$$\frac{\partial \phi}{\partial t} + \left[\frac{dx_E}{dt}\phi\right]_{x_E} = D_u \frac{\partial^2 \phi}{\partial x_E^2} + \frac{\kappa_1}{\Omega} - \phi\kappa_{-1} + \phi^2\psi\kappa_3\Omega^2, \tag{A2}$$

$$\frac{\partial \psi}{\partial t} + \left[\frac{dx_E}{dt}\psi\right]_{x_E} = D_v \frac{\partial^2 \psi}{\partial x_E^2} + \frac{\kappa_2}{\Omega} - \phi^2\psi\kappa_3\Omega^2, \tag{A3}$$

where ϕ and ψ are defined in equations (4) and (5). Converting to Lagrangian coordinates and dropping the L yields

$$\frac{\partial \phi}{\partial t} + \frac{\dot{n}}{n}\phi = \frac{D_u}{n^2}\frac{\partial^2 \phi}{\partial x^2} + \frac{\kappa_1}{\Omega} - \phi\kappa_{-1} + \phi^2\psi\kappa_3\Omega^2, \tag{A4}$$

$$\frac{\partial \psi}{\partial t} + \frac{\dot{n}}{n}\psi = \frac{D_v}{n^2}\frac{\partial^2 \psi}{\partial x^2} + \frac{\kappa_2}{\Omega} - \phi^2\psi\kappa_3\Omega^2. \tag{A5}$$

Finally, by rescaling $\phi_L = \phi n$ and $\psi_L = \psi n$, we remove the dilution terms and, upon ignoring the subscript, L, again, we obtain

$$\frac{\partial \phi}{\partial t} = \frac{D_u}{n^2}\frac{\partial^2 \phi}{\partial x^2} + \frac{\kappa_1 n}{\Omega} - \phi\kappa_{-1} + \frac{\phi^2\psi\kappa_3\Omega^2}{n^2}, \tag{A6}$$

$$\frac{\partial \psi}{\partial t} = \frac{D_v}{n^2}\frac{\partial^2 \psi}{\partial x^2} + \frac{\kappa_2 n}{\Omega} - \frac{\phi^2\psi\kappa_3\Omega^2}{n^2}. \tag{A7}$$

Using this as a template, we redefine the stochastic rates of reaction so as to simulate the reactions on a Lagrangian domain:

$$\emptyset \xrightarrow{\kappa_1 n} U, \quad U \xrightarrow{\kappa_{-1}} \emptyset, \quad \emptyset \xrightarrow{\kappa_2 n} V, \quad 2U + V \xrightarrow{\kappa_3/n^2} 3U. \tag{A8}$$

Thus, the mean-field equations of these reactions (plus diffusion scaled similarly) are exactly Eqs. (A6) and (A7).

Assuming deterministic growth, the stoichiometric matrix is

$$\boldsymbol{\nu} = \begin{bmatrix} \boldsymbol{R} & \boldsymbol{L} & \boldsymbol{0} & \boldsymbol{0} & \boldsymbol{I} & -\boldsymbol{I} & \boldsymbol{0} & \boldsymbol{I} \\ \boldsymbol{0} & \boldsymbol{0} & \boldsymbol{R} & \boldsymbol{L} & \boldsymbol{0} & \boldsymbol{0} & \boldsymbol{I} & -\boldsymbol{I} \end{bmatrix}, \tag{A9}$$

where $\boldsymbol{L}$ and $\boldsymbol{R}$ are the $K \times K$ stoichiometric matrices for diffusion left and right, respectively [see Eqs. (1) and (2)], and I is the $K \times K$ identity matrix. The corresponding vector of macroscopic transition rates, a, is

$$\begin{aligned} \mathsf{a}^T = \Bigg[& \frac{d_1\phi_1}{n^2}, \ldots, \frac{d_1\phi_K}{n^2}, \frac{d_2\psi_1}{n^2}, \ldots, \frac{d_2\psi_K}{n^2}, \frac{n}{\Omega}\kappa_1, \\ & \ldots, \frac{n}{\Omega}\kappa_1, \phi_1\kappa_{-1}, \ldots\ldots, \phi_N\kappa_{-1}, \frac{n}{\Omega}\kappa_2, \\ & \ldots, \frac{n}{\Omega}\kappa_2, \phi_1^2\psi_1\kappa_3\frac{\Omega^2}{n^2}, \ldots, \phi_n^2\psi_n\kappa_3\frac{\Omega^2}{n^2} \Bigg]. \end{aligned} \tag{A10}$$

These then determine the desired matrices $\boldsymbol{A}$ and $\boldsymbol{B}$, which have the forms shown in Eqs. (11) and (12). Noting that we are interested in the homogeneous state, $\phi_i = \phi^*$ and $\psi_i = \psi^*$ for all i, we can write down the elements of the matrices $\boldsymbol{A}$ and $\boldsymbol{B}$ as

$$\begin{gathered} a_1 = \frac{d_1}{n^2}, \quad a_0 = \frac{-2d_1}{n^2} - \kappa_{-1} + 2\phi^*\psi^*\kappa_3\frac{\Omega^2}{n^2}, \\ b_0 = \frac{\phi^{*2}\kappa_3\Omega^2}{n^2}, \\ c_0 = \frac{-2\phi^*\psi^*\kappa_3\Omega^2}{n^2}, \\ d_1 = \frac{d_2}{n^2}, \quad d_0 = \frac{-2d_2}{n^2} - \phi^{*2}\kappa_3\frac{\Omega^2}{n^2}, \quad \alpha_1 = \frac{-2d_1\phi^*}{n^2}, \\ \alpha_0 = \frac{4d_1\phi^*}{n^2} + \frac{n\kappa_1}{\Omega} + \kappa_{-1}\phi^* + \phi^{*2}\psi^*\kappa_3\frac{\Omega^2}{n^2}, \\ \beta_0 = \frac{-\phi^{*2}\kappa_3\psi^*\Omega^2}{n^2}, \\ \gamma_1 = \frac{-2d_2\psi^*}{n^2}, \quad \gamma_0 = \frac{4d_2\psi^*}{n^2} + \frac{n\kappa_2}{\Omega} + \phi^{*2}\psi^*\kappa_3\frac{\Omega^2}{n^2}. \end{gathered}$$

where, for $w \in \{a,b,c,d,e,f,\alpha,\beta,\gamma,\delta\}$, w_0 and w_1 are the diagonal elements and off-diagonal elements of the submatrix $\boldsymbol{w}$, respectively.

In the case that growth is stochastic, the stoichiometric matrix and the macroscopic transition rate vector in Eqs. (A9) and (A10), respectively, will need to be extended in the obvious way. From these we can then calculate the final elements needed to completely define the matrices Eq. (22),

$$\begin{gathered} e_1 = -2\frac{d_u\phi^*}{n^3}, \quad e_0 = \frac{4d_u\phi^*}{n^3} + \frac{\kappa_1}{\Omega} - 2\phi^{*2}\psi^*\kappa_3\frac{\Omega^2}{n^3}, \\ f_1 = -2\frac{d_v\psi^*}{n^3}, \quad f_0 = \frac{4d_v\psi^*}{n^3} + \frac{\kappa_2}{\Omega} + 2\phi^{*2}\psi^*\kappa_3\frac{\Omega^2}{n^3}, \\ \delta_0 = \frac{r}{\theta}. \end{gathered} \tag{A11}$$

[1] P. K. Maini, R. E. Baker, and C. M. Chuong, Science **314**, 1397 (2006).
[2] R. A. Satnoianu and M. Menzinger, Phys. Rev. E **62**, 113 (2000).
[3] W. Zeng, G. L. Thomas, and J. A. Glazier, Physica A **341**, 482 (2004).
[4] R. A. Barrio, R. E. Baker, B. Vaughan Jr., K. Tribuzy, M. R. de Carvalho, R. Bassanezi, and P. K. Maini, Phys. Rev. E **79**, 31908 (2009).
[5] T. E. Woolley, R. E. Baker, P. K. Maini, J. L. Aragón, and R. A. Barrio, Phys. Rev. E **82**, 051929 (2010).
[6] M. R. Owen, J. A. Sherratt, and H. J. Wearing, Dev. Biol. **217**, 54 (2000).
[7] S. Kondo and R. Asai, Nature (London) **376**, 765 (1995).
[8] S. S. Liaw, C. C. Yang, R. T. Liu, and J. T. Hong, Phys. Rev. E **64**, 41909 (2001).
[9] H. Meinhardt, P. Prusinkiewicz, and D. R. Fowler, *The Algorithmic Beauty of Sea Shells* (Springer-Verlag, Berlin, 2003).
[10] A. M. Turing, Phil. Trans. R. Soc. Lond. B **237**, 37 (1952).
[11] C. M. Lin, T. X. Jiang, R. E. Baker, P. K. Maini, R. B. Widelitz, and C. M. Chuong, Dev. Biol. **334**, 369 (2009).
[12] S. Sick, S. Reinker, J. Timmer, and T. Schlake, Science **314**, 1447 (2006).
[13] S. W. Cho, S. Kwak, T. E. Woolley, M. J. Lee, E. J. Kim, R. E. Baker, H. J. Kim, J. S. Shin, P. K. Tickle, C. Maini, and H. S. Jung, Development **138**, 1807 (2011).
[14] T. Biancalani, D. Fanelli, and F. Di Patti, Phys. Rev. E **81**, 046215 (2010).
[15] J. García-Ojalvo and J. M. Sancho, Phys. Rev. E **49**, 2769 (1994).
[16] J. García-Ojalvo and J. M. Sancho, Phys. Rev. E **53**, 5680 (1996).
[17] J. García-Ojalvo and J. M. Sancho, *Noise in Spatially Extended Systems* (Springer-Verlag, Berlin, 1999).
[18] F. Sagués, J. M. Sancho, and J. García-Ojalvo, Rev. Mod. Phys. **79**, 829 (2007).
[19] C. Escudero, J. Stat. Mech. (2009) P07020.
[20] R. E. Baker, C. A. Yates, and R. Erban, Bull. Math. Biol. **72**, 719 (2010).
[21] C. W. Gardiner, *Handbook of Stochastic Methods* (Springer-Verlag, Berlin, 1985).
[22] N. G. van Kampen, *Stochastic Processes in Physics and Chemistry*, 3rd ed. (North-Holland, Amsterdam, 2007).
[23] A. J. McKane and T. J. Newman, Phys. Rev. Lett. **94**, 218102 (2005).
[24] A. J. McKane, J. D. Nagy, T. J. Newman, and M. O. Stefanini, J. Stat. Phys. **128**, 165 (2007).
[25] C. A. Lugo and A. J. McKane, Phys. Rev. E **78**, 51911 (2008).
[26] T. Butler and N. Goldenfeld, Phys. Rev. E **80**, 030902 (2009).
[27] T. Butler and N. Goldenfeld, Phys. Rev. E **84**, 011112 (2011).
[28] T. E. Woolley, R. E. Baker, E. A. Gaffney, and P. K. Maini, Phys. Rev. E **84**, 021915 (2011).
[29] T. E. Woolley, R. E. Baker, E. A. Gaffney, and P. K. Maini, in press.
[30] E. J. Crampin, E. A. Gaffney, and P. K. Maini, Bull. Math. Biol. **61**, 1093 (1999).
[31] A. A. Neville, P. C. Matthews, and H. M. Byrne, Bull. Math. Biol. **68**, 1975 (2006).
[32] I. Barrass, E. J. Crampin, and P. K. Maini, Bull. Math. Biol. **68**, 981 (2006).
[33] S. S. Andrews and D. Bray, Phys. Biol. **1**, 137 (2004).
[34] R. Erban, S. J. Chapman, and P. K. Maini, e-print arXiv:0704.1908v2 [q-bio.SC], 2007.
[35] J. D. Murray, *Mathematical Biology I: An Introduction*, 3rd ed., Vol. 1 (Springer-Verlag, Berlin, 2003).
[36] C. W. Gardiner, K. J. McNeil, D. F. Walls, and I. S. Matheson, J. Stat. Phys. **14**, 307 (1976).
[37] D. A. McQuarrie, J. Appl. Prob. **4**, 413 (1967).
[38] K. W. Morton and D. F. Mayers, *Numerical Solution of Partial Differential Equations: An Introduction* (Cambridge University Press, Cambridge, 2005).
[39] G. Grimmett and D. Stirzaker, *Probability and Random Processes* (Oxford University Press, Oxford, 2001).
[40] T. Jahnke and W. Huisinga, J. Math. Biol. **54**, 1 (2007).
[41] H. Risken, *The Fokker-Planck Equation: Methods of Solution and Applications* (Springer-Verlag, Berlin, 1989).
[42] J. Elf and M. Ehrenberg, Genome. Res. **13**, 2475 (2003).
[43] E. J. Crampin and P. K. Maini, Comm. Theor. Biol. **6**, 229 (2001).
[44] E. J. Crampin, Ph.D. thesis, University of Oxford, 2000.
[45] B. K. Øksendal, *Stochastic Differential Equations: An Introduction with Applications* (Springer-Verlag, Berlin, 2003).
[46] W. L. Briggs and V. E. Henson, *The DFT: An Owner's Manual for the Discrete Fourier Transform* (SIAM, 1995).
[47] F. Zheng-Ping, X. Xin-Hang, W. Hong-Li, and O. Qi, Chin. Phys. Lett. **25**, 1220 (2008).
[48] J. D. Murray, *Mathematical Biology II: Spatial Models and Biomedical Applications*, 3rd ed., Vol. 2 (Springer-Verlag, Berlin, 2003).
[49] D. T. Gillespie, J. Phys. Chem. A **106**, 5063 (2002).
[50] D. T. Gillespie, J. Chem. Phys. **113**, 297 (2000).
[51] D. T. Gillespie, Am. J. Phys. **64**, 1246 (1996).
[52] P. Arcuri and J. D. Murray, J. Math. Biol. **24**, 141 (1986).
[53] P. K. Maini, K. J. Painter, and H. N. P. Chau, J. Chem. Soc. Faraday Trans. **93**, 3601 (1997).
[54] H. Levine and W. J. Rappel, Phys. Rev. E **72**, 061912 (2005).
[55] P. Guptasarma, BioEssays **17**, 987 (1995).
[56] A. Gierer and H. Meinhardt, Biol. Cybern. **12**, 30 (1972).
[57] J. Schnakenberg, J. Theor. Biol. **81**, 389 (1979).